A comprehensive two-hybrid analysis to explore the *L. pneumophila* effector-effector interactome

Harley O'Connor Mount[1]†, Malene L. Urbanus[2]†, Dayag Sheykhkarimli[3,4], Atina G. Coté[3,4], Florent Laval[5,6,7,8,9,10], Georges Coppin[5,6,7,9], Nishka Kishore[3,4], Roujia Li[3,4], Kerstin Spirohn-Fitzgerald[5,6,7], Morgan O. Petersen[2,11], Jennifer J. Knapp[3,4], Dae-Kyum Kim[3,4], Jean-Claude Twizere[8,9], Michael A. Calderwood[5,6,7], Marc Vidal[5,6], Frederick P. Roth[1,3,4,12] and Alexander W. Ensminger[1,2*]

[1]Department of Molecular Genetics, University of Toronto, Toronto, ON, M5G 1M1, Canada.

[2]Department of Biochemistry, University of Toronto, Toronto, ON, M5G 1M1, Canada.

[3]Donnelly Centre, University of Toronto, Toronto, ON, M5G 3E1, Canada.

[4]Lunenfeld-Tanenbaum Research Institute, Sinai Health, Toronto, ON, M5G 1X5, Canada.

[5]Center for Cancer Systems Biology (CCSB), Dana-Farber Cancer Institute, Boston, MA, 02215, USA.

[6]Department of Genetics, Blavatnik Institute, Harvard Medical School, Boston, MA, 02115, USA.

[7]Department of Cancer Biology, Dana-Farber Cancer Institute, Boston, MA, 02215, USA.

[8]TERRA Teaching and Research Centre, University of Liège, 5030, Gembloux, Belgium.

[9]Laboratory of Viral Interactomes, GIGA Institute, University of Liège, 4000, Liège, Belgium.

[10]Laboratory of Molecular and Cellular Epigenetics, GIGA Institute, University of Liège, 4000, Liège, Belgium.

[11]Department of Microbiology and Immunology, The University of Melbourne at the Peter Doherty Institute for Infection and Immunity, Melbourne, VIC 3000, Australia.

23 [12]Department of Computational and Systems Biology, University of Pittsburgh School of
24 Medicine, Pittsburgh, PA, 15260, USA.
25
26 †These authors contributed equally to this work.
27 *Corresponding author:
28 Email: alex.ensminger@utoronto.ca
29
30 **Running title:**
31 **A pathogen effector-effector interactome**
32
33 **Keywords: bacterial effector/host-pathogen/*Legionella pneumophila*/metaeffector/Yeast**
34 **Two-Hybrid**
35
36 **ORC IDs**
37 Harley O'Connor Mount 0000-0003-1401-9178
38 Malene L. Urbanus 0009-0008-0850-3805
39 Dayag Sheykhkarimli 0000-0001-8415-6659
40 Atina G. Coté 0000-0002-0340-9325
41 Florent Laval 0000-0001-7744-6199
42 Georges Coppin 0000-0001-7647-3240
43 Nishka Kishore 0000-0002-9219-4310
44 Kerstin Spirohn-Fitzgerald 0000-0002-2071-1606
45 Morgan O. Petersen 0009-0002-2708-0090

Jennifer J. Knapp 0000-0003-3347-4686

Dae-Kyum Kim 0000-0003-4568-8278

Jean-Claude Twizere 0000-0002-8683-705X

Michael A. Calderwood 0000-0001-6475-1418

Marc Vidal 0000-0003-3391-5410

Frederick P. Roth 0000-0002-6628-649X

Alexander W. Ensminger 0000-0003-0824-3704

Abstract

Legionella pneumophila **uses over 300 translocated effector proteins to rewire host cells during infection and create a replicative niche for intracellular growth. To date, several studies have identified** ***L. pneumophila*** **effectors that indirectly and directly regulate the activity of other effectors, providing an additional layer of regulatory complexity. Amongst these are "metaeffectors" – a special class of effectors that regulate the activity of other effectors once inside the host. A defining feature of metaeffectors is direct, physical interaction with a target effector. Metaeffector identification to date has depended on phenotypes in heterologous systems and experimental serendipity. Using a multiplexed, recombinant-barcode-based yeast two-hybrid technology we screened for protein-protein interactions amongst all** ***L. pneumophila*** **effectors and several components of the Dot/Icm type IV secretion system (>167,000 protein combinations). Of the 52 protein interactions identified by this approach, 44 are novel protein interactions, including ten novel effector-effector interactions (doubling the number of known effector-effector interactions).**

69 **Introduction**

70 Many bacterial pathogens actively translocate protein cargo, called "effectors", into host cells to
71 establish a replicative niche. The perspective that bacterial effectors exclusively target host
72 pathways, and that effector activity is solely regulated by effector expression or translocation
73 timing has been changing with the discovery of functional effector-effector interactions in several
74 bacterial pathogens (Kubori & Nagai, 2011; Shames & Finlay, 2012). The majority of effector-
75 effector interactions described to date are antagonistic but indirect, e.g. one effector antagonizes
76 the action of another effector by acting on host targets. Some indirect antagonists compensate for
77 negative side effects of other effectors (Dean *et al*, 2010) while others act on the same host factor
78 targeted by another effector with opposing actions, e.g. adding and removing post-translational
79 modifications (Kubori & Galán, 2003; Müller *et al*, 2010; Mukherjee *et al*, 2011; Neunuebel *et al*,
80 2011; Tan & Luo, 2011; Tan *et al*, 2011). Effectors in the latter class have the potential to regulate
81 an action on the host in a spatial and/or temporal manner.

82 Cooperative effector interplay has also been identified. For example, paraeffectors LphD
83 and RomA from *Legionella pneumophila,* an intracellular pathogen that is the causative agent of
84 Legionnaires' disease (Fields *et al*, 2002), work consecutively by first deacetylating and then
85 methylating K14 of host histone 3 (Schator *et al*, 2023). *L. pneumophila* effectors LegC2, LegC3,
86 and LegC7 directly cooperate–forming a SNARE-like complex with the human hVAMP4 protein
87 to modulate membrane fusion (Shi *et al*, 2016). Another emerging class of effectors, metaeffectors
88 ("effectors of effectors"), do not target host proteins but instead, once inside the host, directly bind
89 and regulate the activity of other effectors (Kubori *et al*, 2010; Magori & Citovsky, 2011; Urbanus
90 *et al*, 2016; Joseph & Shames, 2021; Bastidas *et al*, 2024).

91 *L. pneumophila* (Fields *et al*, 2002) uses the Dot/Icm Type IVB secretion system (T4SS)
92 to deliver effectors that serve to create a replicative niche in macrophages (Isberg *et al*, 2009) and
93 protozoan species (Fields, 1996; Rowbotham, 1980; Molmeret *et al*, 2005; Faulkner *et al*, 2008;
94 Watanabe *et al*, 2016; Boamah *et al*, 2017; Siddiqui *et al*, 2021). With over 300 effectors (Burstein
95 *et al*, 2009; Huang *et al*, 2011; Zhu *et al*, 2011), *L. pneumophila* has diverse types of effector
96 interplay: 1. indirect antagonist effectors (Müller *et al*, 2010; Neunuebel *et al*, 2011; Mukherjee *et*
97 *al*, 2011; Tan & Luo, 2011; Tan *et al*, 2011; Valleau *et al*, 2018; Gan *et al*, 2019a; Wan *et al*, 2019;
98 Gan *et al*, 2020; Song *et al*, 2021), 2. cooperative paraeffectors (Schator *et al*, 2023), and 3. direct
99 metaeffectors (Kubori *et al*, 2010; Jeong *et al*, 2015; Urbanus *et al*, 2016; Shames *et al*, 2017;
100 Valleau *et al*, 2018; Bhogaraju *et al*, 2019; Black *et al*, 2019; Gan *et al*, 2019b; Joseph *et al*, 2020;
101 Hsieh *et al*, 2021; McCloskey *et al*, 2021; Song *et al*, 2021).
102 We previously used a genetic interaction screen in the yeast *Saccharomyces cerevisiae* to
103 systematically identify *L. pneumophila* functional effector-effector regulation (Urbanus *et al*,
104 2016). Altogether, this approach identified twenty-three effector-effector suppression pairs, in
105 which an antagonist effector suppresses the yeast growth defect caused by a growth-inhibitory
106 effector. We then examined this subset of effectors for protein-protein interactions (PPIs), using
107 pairwise yeast two-hybrid and mammalian LUMIER to identify nine instances of direct
108 metaeffectors. Collectively, this screen and others have identified 11 confirmed and putative
109 metaeffectors in the *L. pneumophila* effector arsenal (Kubori *et al*, 2010; Jeong *et al*, 2015;
110 Urbanus *et al*, 2016; Shames *et al*, 2017; Valleau *et al*, 2018). However, this is clearly not a
111 complete picture of the possible effector-effector interactions and regulatory pairs in this pathogen:
112 for instance, effectors that do not have a conserved host target in yeast will not inhibit yeast growth
113 and would therefore have been missed in our genetic interaction screen. Similarly, the formation

114 of a SNARE-like complex between LegC2, LegC3 and LegC7 with hVAMP4 (Shi *et al*, 2016) is
115 a clear demonstration that not all physical interactions between effectors represent metaeffector-
116 effector regulatory relationships.

117 To complement our previous genetic interaction screen, we performed a systematic screen
118 for physical effector-effector interactions using the Barcode Fusion Genetic-Yeast Two-Hybrid
119 (BFG-Y2H) assay, a high-throughput Y2H approach with a barcode sequencing readout (Yachie
120 *et al*, 2016). Because many *L. pneumophila* effectors inhibit yeast growth when overexpressed
121 (Campodonico *et al*, 2005; Shohdy *et al*, 2005; de Felipe *et al*, 2008; Heidtman *et al*, 2009; Shen
122 *et al*, 2009; Guo *et al*, 2014; Urbanus *et al*, 2016), we modified the Y2H vectors to keep them
123 transcriptionally silent prior to the readout of each potential binding event. This inducible BFG-
124 Y2H (iBFG-Y2H) technology was used to screen for protein interactions between 390 effectors
125 and putative effectors and 28 Dot/Icm T4SS components in >167,000 pairwise combinations.

126

127 **Results**

128 **Modification of a high-throughput yeast two-hybrid approach to reduce loss of yeast-toxic**
129 **genes from screening libraries**

130 To screen all *L. pneumophila* effectors for binary physical interactions, we performed a pooled,
131 multiplexed yeast two-hybrid screen that exploits recombinant DNA barcode pairs to detect binary
132 physical interactions within a library of clones (Yachie *et al*, 2016). Briefly, the BFG-Y2H assay
133 is based on the original Y2H assay (Fields & Song, 1989) in which the yeast transcriptional
134 activator Gal4 is split into a DNA-binding domain (DB) and an activating domain (AD), and each
135 'bait' protein X is fused to DB (DB-X) and each potential 'prey' protein Y is fused to the AD
136 domain (AD-Y). A physically interacting pair of proteins X and Y can thus reconstitute the Gal4

137 protein and drive transcription of reporter genes such as *GAL1::HIS3*, which allows for growth on
138 medium lacking histidine. A key strength of the BFG-Y2H assay is scalability – Y2H screens are
139 performed in multiplexed pools using Illumina sequencing of molecular barcodes as a readout of
140 the pool composition (Yachie *et al*, 2016) (Fig 1A). Each DB-X and AD-Y vector contains a
141 molecular barcode locus with two unique tags ("uptag" and "downtag"), such that one tag is
142 flanked by unique lox sites (*loxP*, *lox2272*). Pools of DB-X and AD-Y barcoded vectors are
143 transformed into yeast cells of opposite mating type. After these cell pools are mated *en masse*,
144 the subsequent diploid pool is subjected to Y2H selection and control growth conditions. Upon
145 induction of Cre-recombinase, lox-flanked tags on reciprocal DB and AD vectors within the same
146 cell are recombined *in vivo*. The resulting chimeric barcodes uniquely identify the DB-X/AD-Y
147 interaction pair, and the abundance of these chimeric barcodes in the sequencing data reflects the
148 abundance of the corresponding strain expressing this interacting pair in the yeast pools (Yachie
149 *et al*, 2016) (Fig 1A).

150 For the purpose of examining physical interactions between *L. pneumophila* effectors, one
151 complication is that standard BFG-Y2H vectors express DB-X and AD-Y using a constitutive
152 *ADH1* promoter, which would express Gal4-domain-fused effector proteins throughout the entire
153 screening process. This is problematic, given that two-thirds of *L. pneumophila* effectors have
154 yeast-growth inhibitory effects that range from severe to mild (Campodonico *et al*, 2005; Shohdy
155 *et al*, 2005; de Felipe *et al*, 2008; Heidtman *et al*, 2009; Xu *et al*, 2010; Belyi *et al*, 2012; Guo *et*
156 *al*, 2014; Nevo *et al*, 2014; Urbanus *et al*, 2016), which likely reflects the conservation of their
157 targets in *S. cerevisiae* (Lesser & Miller, 2001; Campodonico *et al*, 2005; Shohdy *et al*, 2005;
158 Heidtman *et al*, 2009; Xu *et al*, 2010; Tan *et al*, 2011; Belyi *et al*, 2012; Guo *et al*, 2014; Nevo *et*
159 *al*, 2014; Dong *et al*, 2016; Liu *et al*, 2017; He *et al*, 2019).

160 To mitigate the impact of effector-induced growth inhibition, we modified each BFG-Y2H
161 vector by replacing the constitutive *ADH1* promoter with the copper-inducible *CUP1* promoter
162 (Butt & Ecker, 1987). This allowed us to avoid expressing each DB-X and AD-Y fusion during
163 haploid library construction, expansion, and mating of DB- and AD-containing strains. To confirm
164 inducible expression, we grew yeast with 'empty' DB or AD vectors in medium lacking copper to
165 keep expression at a minimum or induced with 1 mM copper for 3, 6 and 24 hours. We observed
166 no expression of the AD or DB domain at T0, or when uninduced, and increasing expression at 3,
167 6 and 24 hours (Fig 1B).

168 Next, we tested five Y2H PPIs between known growth-inhibitory effectors and their
169 corresponding metaeffectors. These pairs had been identified previously by transforming AD-
170 fused toxic effectors to strains already carrying DB-fused metaeffectors (Urbanus *et al*, 2016).
171 Briefly, we mated AD-fused toxic effectors and DB-fused antagonist haploid strains and selected
172 for diploids (containing both AD- and DB-vectors on medium lacking copper). We then queried
173 each diploid strain for the ability to grow under two standard Y2H selective conditions: 1. on
174 medium lacking histidine, and 2. on medium lacking histidine supplemented with 3-AT (an
175 inhibitor of His3p commonly used to increase the stringency of Y2H selection). Of the five pairs,
176 four were captured using the inducible BFG-Y2H vectors (Fig 1C). In agreement with our previous
177 experiments (Urbanus *et al*, 2016), the strongest interaction pairs LegL1-RavJ and MavE-
178 LegC7/YlfA grew well on both selective conditions and the weaker interaction pair LupA-LegC3
179 only supported growth on medium lacking histidine. In a minor deviation from our previous
180 findings using standard Y2H vectors, the fifth metaeffector-effector pair we tested (SidP-MavQ)
181 was only captured under lower stringency conditions (-histidine).

182 Taken together, these data show that the inducible BFG-Y2H vectors are sufficiently
183 transcriptionally silent to perform the BFG-Y2H screening process of transformation, mating and
184 diploid selection and the inducible BFG-Y2H (iBFG-Y2H) assay captures previously known
185 metaeffector-effector pairs with a similar, but not identical, sensitivity profile.
186
187 **An iBFG-Y2H screen of *L. pneumophila* Dot/Icm secretion system components and effectors**
188 To extend this approach to the entire *L. pneumophila* effector arsenal, we combined previously
189 constructed *L. pneumophila* open reading frame (ORF) clones in Gateway vectors (Losick *et al*,
190 2010; Urbanus *et al*, 2016) with clones for an additional 52 effector and putative effector ORFs,
191 collectively assembling clones for 267 confirmed effectors and 123 putative effectors (Table EV1).
192 We also included ORF clones representing 28 components of the Dot/Icm type IV secretion system
193 (T4SS), both as positive controls and to potentially discover Dot/Icm protein interactions with
194 effectors. As a positive reference set of human protein interactions (hsPRS), we included 21 well-
195 characterized human protein pairs known to interact (Table EV2) (Yachie *et al*, 2016). Overall,
196 these AD-Y and DB-X fusion collections contain 435 unique ORFs represented by 1,244 uniquely
197 barcoded iBFG-Y2H vectors, and 422 unique ORFs represented by 1,137 uniquely barcoded
198 iBFG-Y2H vectors, respectively (Table EV1). The majority of ORFs are represented by 3 unique
199 barcode replicates (Fig EV1A, B). Of the 418 *L. pneumophila* effector and Dot/Icm ORFs, 400 are
200 represented in both AD and DB libraries whereas the remaining 18 were only screened in one
201 direction due either to high background ('autoactivation') or other technical limitations (Table
202 EV3). We mated the AD-Y and DB-X haploid collections *en masse* to generate a pool of AD-DB
203 diploid cells (>1.4 million possible unique barcode combinations) and then induced expression
204 using 1 mM copper during growth on control medium and selective medium lacking histidine.

205 Following growth of the pools, the barcodes of the control condition and the Y2H-selective
206 condition were PCR amplified and sequenced (yielding ~54 and ~72 million read pairs,
207 respectively). Each barcode recombination event results in two chimeric barcode combinations
208 (Fig 1A, step 4, 5). To assess if there are barcode specific effects due to PCR or sequencing
209 artifacts, we looked at the correlation of the two chimeric barcodes created during AD-Y and DB-
210 X barcode recombination for both pools (Fig EV1C, D), which showed a strong congruence
211 indicating no major barcode-specific effects.

212 Next, we benchmarked our screen by examining the barcode-fusion data for the 21
213 expected human-human interactions (Table EV2). For each possible X-Y combination in the pool,
214 an interaction score was calculated that reflects the enrichment of the X-Y combination in the
215 Y2H-selective condition over the control condition (Fig 2A) (Yachie *et al*, 2016). At the maximum
216 Matthews correlation coefficient (MCC), which optimizes for a balance of high precision and
217 recall, 20 hsPRS interactions exceeded the corresponding interaction score threshold (Fig 2B,
218 Table EV4), a recall of 95%.

219 Outside of the hsPRS set, 107 Dot/Icm-Dot/Icm, Dot/Icm-effector, effector-effector and
220 human protein-effector interaction pairs exceeded the MCC-optimal threshold. To verify these, we
221 first recloned each gene and created new individual AD and DB strains. After mating, the resulting
222 diploids were spotted onto control medium and Y2H-selective medium and scored for growth after
223 3 days. In total, this retesting verified 56 *L. pneumophila* interaction pairs (Fig 2C, Fig EV2, Table
224 EV4), a retest rate of 52%. For perspective, this is comparable to the ~50% verification rate
225 reported for the original BFG-Y2H screen (Yachie *et al*, 2016) as well as other high-throughput
226 Y2H studies (Rual *et al*, 2005; Yu *et al*, 2008; Simonis *et al*, 2009). Notably, we observed that as
227 the confirmation series approached the MCC-optimal threshold, the Y2H retest-verification rate

228 decreased rapidly, suggesting that the MCC-optimal threshold based on the hsPRS is an
229 appropriate cut-off for *L. pneumophila* interactions (Fig 2C).
230 Taken together, performance of the iBFG-Y2H screen in our hands matched prior
231 expectations. It captured 95% of the human positive reference set, had a verification rate of 52%
232 for the non-hsPRS interactions and identified 56 non-hsPRS interaction pairs representing 52
233 unique PPIs (4 interactions were captured in both the AD-DB and DB-AD orientation) (Table
234 EV4).
235
236 **Validation of iBFG-Y2H interactions by an orthologous (yN2H) assay**
237 To further evaluate the quality of the *L. pneumophila* iBFG-Y2H interaction data, we next turned
238 to the orthogonal yeast-based NanoLuc two-hybrid assay (yN2H) (Choi *et al*, 2019). In this assay,
239 nanoluciferase is split into two fragments: the N-terminal Fragment 1 and C-terminal fragment 2.
240 Enzymatic activity of NanoLuc is reconstituted when the two fragments are brought into close
241 proximity by interacting fusion partners. We created copper-inducible N2H vectors to assay *L.*
242 *pneumophila* PPIs in the yN2H assay. We measured the N2H signals of 33 retest-positive *L.*
243 *pneumophila* interaction pairs as N1-X:N2-Y and N1-Y:N2-X fusions along with a set of well-
244 described interactions (positive reference set, hsPRS-v2) and randomly selected pairs (random
245 reference set, hsRRS-v2) (Venkatesan *et al*, 2009; Rolland *et al*, 2014; Choi *et al*, 2019; Luck *et*
246 *al*, 2020) cloned into the standard N2H vector (Choi *et al*, 2019) (Table EV5). The detection rate
247 for the *L. pneumophila* interactions pairs in a single orientation was compared to the detection rate
248 of the hsPRS-v2 and hsRRS-v2 (Choi *et al*, 2019) (Fig 3A). The detection threshold was set at the
249 normalized luminescence ratio (NLR) value where the hsRRS-v2 distribution has a Z-score >2.23
250 and the probability of the hsRRS-v2 values to be below the threshold is 98.7%. The N2H detection

251 rate of our dataset was 48.5 % which exceeds the hsPRS-v2 set detection rate of 18.3 % (Fig 3B),
252 so that we can consider our entire interaction dataset to be well validated. Indeed, by this measure,
253 the quality of the verified *L. pneumophila* iBFG-Y2H interactome exceeds that of a high-quality
254 interaction dataset supported by multiple experiments in the curated literature (Braun *et al*, 2009;
255 Venkatesan *et al*, 2009; Rolland *et al*, 2014; Choi *et al*, 2019; Luck *et al*, 2020).
256
257 **The iBFG-Y2H screen identifies both known and novel Dot/Icm complex interactions**
258 Returning to the biology of *L. pneumophila* interactions, we first looked at components of the
259 Dot/Icm T4SS. The interaction score heatmap of the 27 DB- and 28 AD-fused Dot/Icm
260 components present in the screen shows nine interaction pairs above the MCC-optimal threshold
261 and verified in the iBFG-Y2H retest assay (Fig 4A, Fig EV2, Table EV4). We expected to see
262 three interactions; IcmQ-IcmR (Duménil & Isberg, 2001), IcmS-IcmW (Coers *et al*, 2000; Ninio
263 *et al*, 2005; Xu *et al*, 2017) and LvgA-IcmS (Vincent & Vogel, 2006; Kim *et al*, 2020), which
264 have all been detected using several PPI assays, including the Y2H assay. IcmQ-IcmR and IcmS-
265 IcmW were captured in both directions (Fig 4B) above the MCC-optimal threshold and verified in
266 the iBFG-Y2H retest assay, but the LvgA-IcmS pairs were below the MCC-optimal threshold and
267 were thus not further tested or assessed by N2H. Of the five additional verified PPIs from the
268 iBFG-Y2H assay, three are supported by previously published data: DotB-DotB, IcmG/DotF-
269 IcmG/DotF and DotC-IcmG/DotF (Fig 4B). The ATPase DotB can be purified as hexamer (Sexton
270 *et al*, 2004), IcmG/DotF was shown to self-associate using the BACTH assay (Vincent *et al*, 2006)
271 and DotC and IcmG/DotF are both part of the T4SS core complex (Vincent *et al*, 2006). The
272 remaining two PPIs: IcmB/DotO-IcmT and IcmV-IcmG/DotF, are novel.

273 In contrast to a previous Y2H study identifying interactors of IcmW (Ninio *et al*, 2005),
274 our assays did not identify any effector interactions with any of the components responsible for
275 transferring effectors to the core transmembrane complex. This transfer is the function of the Type
276 IV coupling complex (T4CC) of which several components are present in the iBFG-Y2H library
277 (IcmO/DotL, IcmP/DotM, IcmJ/DotN, DotY, IcmS, IcmW and LvgA) (Vincent *et al*, 2012;
278 Sutherland *et al*, 2012; Kwak *et al*, 2017; Xu *et al*, 2017; Meir *et al*, 2018, 2020). However, we
279 did find interactions of effectors with Dot/Icm components that are part of the core complex
280 spanning the inner membrane, periplasm and outer membrane: IcmG/DotF, IcmN/DotK,
281 IcmE/DotG and DotC (Fig 4C, Fig EV2, Table EV4) (Vincent *et al*, 2006; Ghosal *et al*, 2019;
282 Durie *et al*, 2020). Notably, IcmG/DotF was previously shown to interact with effectors in BACTH
283 assays (Luo & Isberg, 2004; Sutherland *et al*, 2013) though the relevance of these interactions is
284 unclear (Sutherland *et al*, 2013).
285 Taken together, we captured several known interactions from the Dot/Icm T4SS,
286 uncovered two novel Dot/Icm interactions: IcmB/DotO-IcmT, IcmV-IcmG/DotF and several
287 effector-Dot/Icm T4SS interactions.
288
289 **iBFG-Y2H identifies several novel effector-effector interactions**
290 Next, we looked at effector-effector interactions verified in the iBFG-Y2H retest assay (Fig 5, Fig
291 EV2, Table EV4). The screen captured eleven effector homodimers (Fig 5A), of which only WipA
292 had previously been shown to dimerize (Pinotsis & Waksman, 2017). Beyond this, we identified
293 thirteen physical interactions between pairs of distinct effectors (Fig 5B). These include the
294 published effector-metaeffector pairs RavJ-LegL1 (in both directions) and LegC7/YlfA-MavE
295 (Urbanus *et al*, 2016), consistent with the results of our pilot experiment (Fig 1C). Ten PPIs are

296 novel effector-effector pairs. Of these, three contain a core (conserved) effector – RavC, CetLP1
297 or Lpg2832 (Burstein *et al*, 2016; Gomez-Valero *et al*, 2019) – and three have at least one effector
298 with some characterization: Lpg2149-VipA (Franco *et al*, 2012; Bugalhão *et al*, 2016; Valleau *et*
299 *al*, 2018), PieF-LegK2 (Hervet *et al*, 2011; Michard *et al*, 2015; Mount *et al*, 2022) and WipA-
300 Lpg2860 (He *et al*, 2019; Jia *et al*, 2018; Pinotsis & Waksman, 2017). The remaining four pairs
301 identified in our screen consist of completely uncharacterized effectors and putative effectors.
302

303 **An incidental consequence of the human positive reference set: identification of several**
304 **effector-host interactions**

305 While our screen focused on effector-effector interactions, one consequence of using a set of
306 evolutionary conserved human proteins to benchmark a pooled interaction screen was the
307 fortuitous scoring of interactions between effectors and these conserved host proteins. Several
308 proteins of the hsPRS, which contains conserved eukaryotic proteins such as proteins involved in
309 cell cycle regulation or mRNA degradation, were also found to interact with *L. pneumophila*
310 effectors. We identified 17 effector-human protein pairs (Fig 6, Fig EV2, Table EV4): 8 effectors
311 interact with transcription factor Ikaros (IKZF1) (Fig 6A) and the remaining 9 pairs involve 6
312 different effectors and 7 human proteins (Fig 6B). Of these interactions, 16 are novel and only the
313 PieF-CNOT7 interaction was reported previously (Mount *et al*, 2022).
314

315 **A high-confidence effector interaction network**

316 Using iBFG-Y2H, two novel Dot/Icm-Dot/Icm interactions, six novel effector-Dot/Icm
317 interactions, ten novel effector dimers, ten novel effector-effector interactions and 17 novel
318 effector-human protein interactions were identified. These PPIs and previously published PPIs

319 captured in the iBFG-Y2H screen are visualized in a network (Fig 7), where nodes of published
320 interactions are coloured blue. Examination of this network shows that while most effectors only
321 interact with one other effector or human protein, a few effectors standout as interacting with
322 several different proteins: PieF (interacting with IKFZ1, CNOT7, CDK4, LSM3 and LegK2),
323 VipA (with CDK4 and Lpg2149), Lpg2885 (with Lpg1822 and CetLP1) and MavA (with IKZF1,
324 MRFAP1L1 and AVR58-05830).
325

326 **Discussion**

327 With over >300 effectors, *L. pneumophila* has the largest described bacterial effector arsenal
328 (Ensminger, 2016) with several observed instances of effector interplay that finetune effector
329 function and the progression of pathogenesis (Kubori *et al*, 2010; Müller *et al*, 2010; Neunuebel
330 *et al*, 2011; Tan *et al*, 2011; Tan & Luo, 2011; Mukherjee *et al*, 2011; Jeong *et al*, 2015; Urbanus
331 *et al*, 2016; Shames *et al*, 2017; Valleau *et al*, 2018; Gan *et al*, 2019a; Wan *et al*, 2019; Gan *et al*,
332 2020; Schator *et al*, 2023). We previously performed the first genetic interaction screen of bacterial
333 effectors, where we expressed every possible combination of *L. pneumophila str. Philadelphia 1*
334 effectors in the budding yeast *S. cerevisiae* and identified several suppression pairs, where an
335 antagonist effector suppressed the yeast-growth defect caused by a growth-inhibitory effector
336 (Urbanus *et al*, 2016). These suppression pairs were enriched for metaeffectors – effectors that
337 directly target other effectors and regulate their activity in the host cell. Collectively, the field has
338 identified 11 *L. pneumophila* metaeffectors to date (Kubori *et al*, 2010; Urbanus *et al*, 2016;
339 Shames *et al*, 2017; Valleau *et al*, 2018). We reasoned that our genetic interaction screen did not
340 capture all metaeffectors or effectors otherwise functioning in a physical complex (Shi *et al*, 2016).
341 To complement our previous work, we set out to screen all possible effector-effector physical

342 interactions using iBFG-Y2H, a high-throughput, multiplexed protein interaction screen with
343 inducible expression and barcoded vectors for a sequencing readout.

344 In this study, we present the systematic physical interaction screen of a large bacterial
345 pathogen effector arsenal, encompassing 390 *L. pneumophila* effectors and putative effectors and
346 28 Dot/Icm components. We identified 52 interactions between *L. pneumophila* effectors, Dot/Icm
347 T4SS components, and effectors with Dot/Icm T4SS components or human proteins. A subset
348 iBFG-Y2H PPIs were detected in the orthologous NanoLuc Two-Hybrid (N2H) assay (Choi *et al*,
349 2019) at a rate of 48.5% (Fig 3). This is better than the detection date for a high-quality positive
350 reference set, indicating that the verified iBFG-Y2H set – with 16 PPIs captured in both assays –
351 is a high-confidence dataset. Our screen captured several known interactions between components
352 of the Dot/Icm T4SS system (Coers *et al*, 2000; Duménil & Isberg, 2001; Sexton *et al*, 2004; Ninio
353 *et al*, 2005; Vincent *et al*, 2006; Xu *et al*, 2017; Kim *et al*, 2020), the WipA dimer (Pinotsis &
354 Waksman, 2017) two of our previously published effector-metaeffector pairs; RavJ-LegL1 and
355 LegC7/YlfA-MavE (Urbanus *et al*, 2016) and PieF-CNOT7 (Mount *et al*, 2022) (Fig 7). The ten
356 novel effector-effector interactions involve 19 effectors, approximately 5% of the total effectors,
357 and doubles the number of known PPIs between *L. pneumophila* effectors. This reinforces the
358 notion that bacterial effectors do not act on their own and need to be studied in concert rather than
359 in isolation.

360 The functional consequences of the effector-effector interactions we identified remain to
361 be defined. They may represent metaeffector-effector pairs, effectors functioning in a complex, or
362 some other functional relationship yet to be discovered. Nevertheless, these physical interactions
363 already suggest interesting functional links. For example, Lpg2149 links the actin nucleator VipA
364 (Franco *et al*, 2012) with modulators of the E3 ubiquitin ligase UBE2N, MavC and MvcA. As

365 previously reported, MavC modifies and inactivates UBE2N (Valleau *et al*, 2018; Gan *et al*, 2019a,
366 2020) and MvcA removes that modification (Gan *et al*, 2020; Wang *et al*, 2020). Lpg2149 is the
367 metaeffector of MavC and MvcA, and inactivates both effectors (Valleau *et al*, 2018). Notably,
368 UBE2N has been shown to be involved in ubiquitination of β-actin (Chua *et al*, 2018) and is
369 recruited to actin-rich structures in *Listeria monocytogenes* infections (Chua *et al*, 2023).

370 A fortuitous consequence of including the human positive reference set in our screen was
371 the detection of several novel host protein-effector interactions. The transcription factor Ikaros
372 (IKZF1) stands out, as it interacts with a striking number of effectors. Ikaros is involved in
373 regulation of the host response to bacterial LPS (Oh *et al*, 2018) and hypomorphic Ikaros alleles
374 leave patients at high risk for viral and bacterial infections (Kuehn *et al*, 2022). This raises the
375 question of whether one or more of these effectors modulate Ikaros-regulated host defenses.
376 Indeed, *L. pneumophila* has been shown to target other immune related transcription factors such
377 as NF-κB (Ge *et al*, 2009; Losick *et al*, 2010). We also identified an effector, Ceg29, that may be
378 linked to the TNF signalling pathway known to restrict to restrict *L. pneumophila* growth (Liu *et*
379 *al*, 2008; Pollock *et al*, 2023): Ceg29 interacts with the proteasome non-ATPase regulatory subunit
380 2, PSMD2, which can bind to TNF receptor and is implicated in TNF signalling (Boldin *et al*,
381 1995; Dunbar *et al*, 1997).

382 Two other human protein-effector PPIs that can be linked to known processes during *L.*
383 *pneumophila* infection are: 1) AP2B1-Lem2; and 2) SH3GLB2 (Endophillin B2)-Ceg7. AP2B1 is
384 a component of the clathrin adaptor complex, AP2, and is involved in endocytosis, while
385 Endophillin B2 facilitates endosome maturation. Both processes are heavily targeted by *L.*
386 *pneumophila* as it evades host defenses and maturation of the host phagosome (Finsel & Hilbi,
387 2015). Interestingly, the AP2 complex is also targeted by an effector of *Coxiella burnetii* (Larson

388 *et al*, 2013) a related bacterial pathogen with an intracellular lifestyle. Finally, during infection *L.*
389 *pneumophila* blocks the host cell cycle progression in an effector-dependent manner (Mengue *et*
390 *al*, 2016; Sol *et al*, 2019). Two effectors, VipA and PieF, were found to interact with the cyclin
391 dependent kinase CDK4 suggesting that they could be involved in cell cycle regulation.

392 In summary, our iBFG-Y2H screen of all *L. pneumophila* effectors captured a novel set of
393 PPIs, which builds on and expands our knowledge of the molecular interactions between *L.*
394 *pneumophila* effectors that facilitate *L. pneumophila* pathogenesis. Our dataset doubles the number
395 of known effector-effector interactions and shows that effector-effector interactions and effector
396 interplay are common, rather than an exception. We herein present this dataset as a resource to the
397 field. The next steps in studying these interactions, such as investigating the role of these
398 interactions during host infection, will undoubtedly lead to novel biology and a greater
399 understanding of regulation of pathogenesis of intracellular bacterial pathogens.

400

401 **Methods**

402 *Strains and culture conditions*

403 *Escherichia coli* strain Top10 was used for cloning and plasmid production and grown in LB Miller
404 or 2X LB Miller. *S. cerevisiae* strains RY1010 (MATa *leu2-3,112 trp1-901 his3-200 ura3-52*
405 *gal4Δ gal80Δ PGAL2-ADE2 LYS2::PGAL1-HIS3 MET2::PGAL7-lacZ cyh2^R can1Δ::PCMV-*
406 *rtTA-KanMX4)*, RY1030 (*MATα leu2-3,112 trp1-901 his3-200 ura3-52 gal4Δ gal80Δ PGAL2-*
407 *ADE2 LYS2::PGAL1-HIS3 MET2::PGAL7-lacZ cyh2^R can1Δ::TADH1-PtetO2-Cre-TCYC1-*
408 *KanMX4*) (Yachie *et al*, 2016), Y8800 (MATa) and Y8930 (MATα) (genotype: *leu2-3,112 trp1-*
409 *901 his3-200 ura3-52 gal4Δ gal80Δ PGAL2-ADE2 LYS2::PGAL1-HIS3 MET2::PGAL7-lacZ*
410 *cyh2^R)* were grown in YPAD medium (2% bacto peptone w/v, 1% yeast extract w/v, 2% glucose

411 v/v, 180 mg/l adenine) or synthetic complete (SC) medium lacking specific amino acids with 2%
412 glucose and 180 mg/l adenine. The SC medium for copper inducible strains was prepared using
413 yeast nitrogen base (YNB) without amino acids or copper (ForMedium, catalog # CYN0905).

414

415 *Inducible BFG-Y2H vectors*

416 The constitutive *ADH1* promoter in the BFG-Y2H vectors pNZM1090 and pNZM1100 (Yachie *et*
417 *al*, 2016) was replaced with the *CUP1* promoter sequence (Butt & Ecker, 1987). First, a second
418 HindIII site in pNZM1090 was removed by introducing synonymous substitutions (in the *TRP1*
419 gene) with QuikChange (Agilent) per manufacturer's instructions using primers pNZM1090F and
420 pNZM1090R (Table EV6) resulting in pNZM1090-HindIII. The *CUP1* promoter was amplified
421 from *S. cerevisiae* BY4741 genomic DNA (Brachmann *et al*, 1998) using primers AE897 and
422 AE898, the resulting PCR product was digested with ApaI/HindIII and ligated into ApaI/HindIII
423 digested pNZM1090-HindIII and pNZM1100. The resulting vectors pNZM1090CUP1 and
424 pNZM1100CUP1 were Sanger sequence verified.

425 Inducible expression was tested by growing RY1010 pNZM1090CUP1 and RY1030
426 pNZM1100 strains on SC medium lacking tryptophan or leucine, respectively. Overnight cultures
427 were diluted to 1 OD_{600nm}/ml and induced with or without 1 mM $CuSO_4$. Three OD_{600nm} units were
428 harvested at 0, 3, 6 and 24 h. Samples were lysed as described previously (Zhang *et al*, 2011) and
429 resuspended in 100 µl 2X sample buffer (4% SDS, 20% glycerol, 120 mM Tris pH6.8). The
430 equivalent of 0.3 OD units was analyzed by SDS-PAGE and western blot using the following
431 antibodies and dilutions: mouse anti-AD (Abcam, catalog # ab135398) 1:200 in 3% BSA in PBS-
432 0.5% Tween (PBS-T), mouse anti-DB (Abcam, catalog # ab135397) 1:1000 in 3% BSA in PBS-
433 T, rabbit anti-actin (MilliporeSigma, catalog # A2066) 1:2500 in 5% milk PBS-T and secondary

434 antibodies anti-mouse HRP (1:5000 for anti-AD, and 1:10,000 for anti-DB in 5% milk PBS-T)
435 and anti-rabbit HRP (1:10,000 in 5% milk PBS-T) (Cell Signaling Technology, catalog # 7076
436 and 7074).
437
438 *Barcoded iBFG-Y2H plasmid collection*
439 Randomly barcoded iBFG-Y2H vectors were made as described previously (Yachie *et al*, 2016)
440 with the modification that the barcode cassette was inserted at the SacI site downstream of the
441 Gateway cassette.
442 A Gateway pDONR221 library containing confirmed and putative *L. pneumophila*
443 effectors described previously (Losick *et al*, 2010; Urbanus *et al*, 2016) was a kind gift from Dr.
444 Ralph Isberg. We cloned an additional 52 effectors and putative effectors and 26 Dot/Icm
445 components. ORFs were amplified from genomic DNA from *L. pneumophila* strain Lp02 (Rao *et*
446 *al*, 2013) using the primers listed in Table EV6. The PCR products were cloned into pDONR221-
447 ccdB (Invitrogen) using Gateway BP clonase II (Invitrogen) per manufacturer's instructions and
448 the resulting vectors were sequence verified. The pDONR221 library was cloned *en masse* using
449 Gateway LR Clonase II (Invitrogen) into randomly barcoded iBFG-Y2H vectors. A set of 34
450 human ORFs (Table EV2) for calculation of precision, recall and Mathew's correlation coefficient
451 (MCC) values was included as described (Yachie *et al*, 2016).
452 The randomly barcoded pools were transformed into chemically competent Top10 *E. coli*
453 cells and transformants were arrayed in 384-well format using an S&P robotic rearrayer (S&P
454 Robotics). Barcode and ORF sequences for each clone were determined by kiloSEQ (seqWell Inc).
455 Up to three independent clones (with unique barcodes) were chosen for each ORF. Missing ORFs
456 were cloned individually into randomly barcoded iBFG-Y2H vector pools and transformed into

457 Top10 *E. coli*, and six clones were selected and arrayed into 96-well plates. The barcodes were
458 sequenced using pooled Illumina sequencing with row-column-plate barcodes to link vector
459 barcodes to a unique plate and well identity (Yachie *et al*, 2016). Briefly, *E. coli* cultures were
460 grown overnight in LB medium with 100 µg/ml carbenicillin at 37ºC with shaking in 96-well plates
461 and diluted 1/20 in ddH_2O. Ten microliter row-column PCR reactions were performed with 1 µl
462 barcoded primer corresponding to row A-H and 1 µl barcoded primer for column 1-12 barcoded
463 primer (oHM106-199) (2 µM stock), 5 µl of KAPA HiFi 2X master mix (Roche) and 3 µl of
464 diluted overnight culture grown in 96-well plates. Following PCR amplification, the amplicons
465 from a 96-well plate are pooled and purified using a 2% E-Gel SizeSelect II agarose gel
466 (Invitrogen) and quantified on a NanoDrop spectrophotometer (ThermoFisher Scientific). Purified
467 amplicon pools then underwent a second PCR amplification adding Illumina flow cell adapters as
468 well as additional inline plate barcode sequences (primers oHM146-147, oHM200-213). For each
469 plate, a 40 µl KAPA HiFi reaction was assembled using 1 µl of each primer (oHM200-213, 10 µM
470 stock) and 5 µl of amplicons (1 ng/µl) and purified as above. The purified products were quantified
471 using the NEBNext Library Quant kit for Illumina (NEB) and sequenced using a mid-output
472 reagent cartridge with 2x150 paired-end reads on an Illumina Miniseq platform. Reads were
473 demultiplexed using a custom Perl script (Yachie *et al*, 2016) and aligned to vector sequence using
474 BLAST+ (Camacho *et al*, 2009) to extract barcode identities. Up to three independent clones were
475 selected for each ORF. Plasmid pools were purified from the final arrayed *E. coli* collections using
476 PureYield Plasmid Midipreps (Promega).
477
478 *iBFG-Y2H screen*

479 The iBFG-Y2H screen was performed using the *S. cerevisiae* BFG-Y2H toolkit strains RY1010
480 and RY1030 strains (Yachie *et al*, 2016). Frozen competent yeast cells were prepared as described
481 (Gietz & Schiestl, 2007a) and transformed as follows: 2 ml of frozen competent RY1010 or
482 RY1030 cells were thawed, pelleted and resuspended in an 8.280 ml yeast transformation mixture
483 (33% PEG3350, 0.1 M lithium acetate, 0.3 mg/ml boiled salmon sperm DNA) with 40 µg of the
484 AD or DB iBFG-Y2H vector pool and heat-shocked at 42ºC for 1 h. The cells were pelleted at
485 1000x*g* for 5 min, washed once with 10 ml ddH_2O, re-suspended in ~1ml ddH_2O and plated on
486 eight 15 cm plates of SC medium lacking tryptophan (-Trp for AD vectors), or lacking leucine (-
487 Leu for DB vectors) using YNB without copper. Transformants were grown at 30ºC for 3 days,
488 before being scraped from the plates with ddH_2O and pooled. AD and DB pools were pelleted,
489 washed twice with 25 ml of ddH_2O and resuspended to 100 OD_{600nm} units/ml. To mate, equal
490 volumes (30 ml) of the AD and DB pools were combined and incubated for 3 h at room temperature
491 (RT) without shaking (Bickle *et al*, 2006). The cells were pelleted, resuspended in 1.5 ml of ddH_2O
492 and plated on ten 15 cm YPAD plates and incubated at RT for 3 days. The mated yeast pool was
493 scraped, pelleted and washed twice and resuspended in ddH_2O to 50 OD_{600nm}/ml. The mated pool
494 was plated on eighteen 15 cm plates (200 µl per plate) of Y2H selective medium (SC-Leu/Trp/His
495 + 1 mM $CuSO_4$) or diploid selective medium (SC-Leu/Trp) supplemented with 1 mM $CuSO_4$ and
496 8 mM excess of histidine and incubated at 30ºC for 3 days. For each condition, the plates were
497 then scraped, pooled, washed twice with ddH_2O, and diluted to 1 OD_{600nm}/ml in 100 ml of diploid
498 selective media without $CuSO_4$ and with 10 µg/ml of doxycycline to induce Cre-recombinase
499 expression. To allow *in vivo* Cre-mediated recombination of barcodes the culture was grown
500 overnight at 30ºC with 200 rpm shaking until the OD_{600nm} exceeded 5. Plasmids pools were isolated
501 using the Zymoprep II yeast plasmid miniprep kit (Zymo Research). The fused DNA barcode

502 sequences were amplified using KAPA HiFi 2x master mix and fusion specific primer pairs for
503 each treatment (oHM380-387). For each condition, twenty 40 µl reactions were run with 2 ng of
504 DNA template per reaction to reduce sampling error and pooled together. The primers were used
505 at 10 µM and contained adapters for the Illumina flow cell as described (Yachie *et al*, 2016). The
506 PCR amplicon pools were then purified using 0.7X AMPure magnetic beads (Beckman Coulter)
507 following the Illumina Nextera XT recommendations. The concentration of the purified amplicons
508 was quantified by qPCR using the NEBNext Illumina Quant kit (NEB). The forward and reverse
509 reads were demultiplexed and fused barcodes were quantified through alignment against custom
510 barcode and primer sequences using Bowtie2 (V2.3.4.1) (-q –local –very-sensitive-local -t -p 23 -
511 reorder) (Langmead & Salzberg, 2012).
512
513 *Interaction score calculation*
514 Interaction scores were calculated as described previously (Yachie *et al*, 2016). Briefly, (i) a
515 constant value of 1 was added to every AD-DB barcode combination in both the selective (-
516 Leu/Trp/His + 1 mM $CuSO_4$) and non-selective (-Leu/Trp + 1 mM $CuSO_4$/8 mM His) matrices.
517 (ii) The marginal frequency of each AD or DB clone within the population was determined by
518 dividing the sum of barcode counts for all clones that contain that barcode in the non-selective
519 condition by the sum of all barcode counts in the non-selective matrix. The expected frequency of
520 any AD-DB combination is the product of each clone's marginal frequency in the non-selective
521 condition. (iii) To score enrichment in the selective condition, the frequency of each AD-DB
522 combination was calculated by dividing barcode count for every AD-DB combination by the sum
523 of all barcode counts in the selective matrix. Raw score values (S) were then determined by
524 dividing the selective frequency by the expected marginal frequency product determined in (ii).

525 (iv) Autoactivation was normalized across each DB clone. First, the median value of all S values
526 for each DB clone was subtracted from each raw score (S) giving a new value (S^o). S^o was then
527 divided by the S value that encompasses 60% of all interactions for that DB clone resulting in the
528 interaction score S'. For each AD-DB pair multiple S' scores were calculated based on the number
529 of barcodes for each clone in the pool and the two chimeric barcodes for each AD-DB combination.
530 Through systematic determination, we found that the optimal Matthews Correlation Coefficient
531 (maximizing precision and recall) where MCC optimal = 0.9 was achieved with a threshold where
532 the top 60% of interactions were included in the normalization (ρ=0.4) and the average of the top
533 8 S' signals was adopted.
534
535 *Pairwise retesting of iBFG-Y2H candidate interactions.*
536 Of the 140 PPI pairs above the MCC-optimal rank, we retested 107 pairs involving Dot/Icm-
537 Dot/Icm pairs, effector-Dot/Icm pairs, effector-effector pairs and effector-human protein pairs.
538 Validated Gateway Entry clones were recloned into unbarcoded pNZM1090CUP1 and
539 pNZM1100CUP1 vectors using Gateway LR Clonase II (Life Technologies) per manufacturer's
540 instructions, transformed to RY1010 and RY1030 as described (Gietz & Schiestl, 2007b) and
541 grown for 2 days at 30°C on SC-Trp or SC-Leu agar plates. The resulting haploid strains were
542 arrayed in a 96-well format as an DB (RY1030 pNZM1100CUP1) and AD (RY1010
543 pNZM1090CUP1) array. Using an S&P pinning robot (S&P robotics) the DB and AD arrays were
544 pinned together on YPAD agar plates, incubated overnight at 30°C and diploid strains carrying
545 both plasmids were pinned on SC-Leu/Trp agar plates and grown for 2 days at 30°C. An empty
546 vector control was included on each array plate. To check for autoactivator activity, the DB and
547 AD arrays were mated to an AD or DB empty vector control strain, respectively. The resulting

548 diploid plates were grown overnight in 100 µl SC-Leu/Trp medium in 96-well plates at 30°C,
549 diluted 10-fold in fresh medium and spotted on SC-Leu/Trp (control), SC-Leu/Trp/His + 1 mM
550 $CuSO_4$ (Y2H selective condition) agar plates using a 96-well pin tool (V&P404, V&P Scientific)
551 and grown for 3 days at 30°C before imaging (Fig EV2, Table EV4). The retest positive pairs were
552 subsequently tested on two Y2H selective conditions: SC-Leu/Trp/His+ $CuSO_4$ and the more
553 stringent condition with 1 mM 3-AT to assess the strength of the interactions and to assay clones
554 with autoactivator activity.
555
556 *Pairwise validation of L. pneumophila effector interactions by yN2H assay*
557 The promoter sequence of the NanoLuc Two-Hybrid (N2H N1 & N2) vectors (Choi *et al*, 2019)
558 was replaced with the *CUP1* promoter. The *CUP1* promoter sequence was amplified from the
559 iBFG-Y2H vectors (primers oHM487/488) and cloned into N2H N1 and N2 vectors digested with
560 SpeI/SacI using NEBuilder assembly (NEB) according to manufacturer's instructions. The
561 resulting vectors pHM526 and pHM527 were Sanger sequence verified.
562 ORFs from the iBFG-Y2H-verified set were cloned into iN2H pDEST vectors using LR
563 Clonase II as described above. Bacterial transformants were grown overnight in LB + carbenicillin
564 (100 µg/ml), 200 µl of culture was pelleted and resuspended in 130 µl. Fifteen microliters of cell
565 suspension was incubated for 30 min at 27ºC with 15 µl of 2x bacterial lysis buffer (2 mg/ml
566 lysozyme, 20 mM Tris-HCl pH 6.8, 2 mM EDTA). The lysates were incubated for 20 mins at 55ºC
567 with 5 µl of proteinase K mixture (12 mg/ml proteinase K, 20 mM Tris-HCl, 2 mM EDTA)
568 followed by 20 mins at 80ºC to inactivate proteinase K. Competent yeast cells (Y800 and Y8930)
569 were prepared as described (Gietz & Schiestl, 2007b) 20 µl of competent Y8800 or Y8930 cells
570 was pelleted, resuspended in 148 µl of yeast transformation mix and combined with 15 µl of lysate

571 for transformation. Transformations were incubated for 30 mins at 42ºC, pelleted and resuspended
572 in 100 µl of YPAD. Resuspended yeast cells were recovered for 2 h at 30ºC washed with 100 µl
573 of ddH_2O, resuspended in 10 µl of ddH_2O, plated onto selective media (SC-Leu or SC-Trp) and
574 incubated for 3 days at 30ºC.

575 The yN2H assay was performed as described (Choi *et al*, 2019) with minor modifications.
576 Briefly, Y8930 with pHM526 (N1/Fragment 1, *LEU2* cassette) or Y8800 + pHM527
577 (N2/Fragment 2 vectors, *TRP1* cassette) were grown overnight in 160 µl SC-Leu or SC-Trp
578 medium at 30°C in a 96-well plate. A positive and random reference set (hsPRS-v2 and hsRRS-
579 v2) in original N2H vectors (Choi *et al*, 2019) were grown in parallel. Two protein pairs from the
580 hsPRS-v2 (SKP1-SKP2; NCBP1-NCBP2) were included in duplicate on every test plate and used
581 as positive controls. Mating was performed by mixing 5 µl of each Y8930 and Y8800 strain in a
582 96-well plate containing 160 µl YPD medium per well and incubated overnight at 30ºC. Strains
583 expressing *L. pneumophila* ORF fusions were also mated with a control strain expressing only
584 Fragment 1 (N1) or Fragment 2 (N2) to measure the background signal (e.g. N1-X was mated with
585 N2-Y, where X and Y are the proteins tested for interaction, as well as Fragment 2 alone). To
586 select for diploid strains, 10 µl of the mating mixture was grown overnight in 160 µl SC-Leu/Trp
587 at 30°C in 96-well plates. Fifty microliters of the diploid selection cultures were transferred into
588 1.2 ml of fresh medium (SC-Leu/Trp) in deep 96-well plates. Plates were grown overnight at 30ºC
589 with shaking, cultures were pelleted (1,800xg for 15 min) and resuspended in 100 µl NanoLuc
590 Assay solution (Promega). The homogenized cell suspensions were transferred into white flat-
591 bottom 96-well plates and incubated for 1 h at RT while protected from light. The luminescence
592 signal was measured using a TriStar2 LB 942 luminometer (Berthold) with a one-second orbital
593 shake before each measurement and an integration time of 2 s per sample.

594 For each protein pair X-Y, we calculated a normalized luminescence ratio (NLR)
595 corresponding to the raw luminescence value of the tested pair (X-Y) divided by the maximum
596 luminescence value from one of the two controls (X-Fragment 2 or Fragment 1-Y) (Choi *et al*,
597 2019). The log-transformed NLR was plotted for human positive and random reference sets
598 previously used with N2H (hsPRS-v2 and hsRRS-v2) and verified iBFG-Y2H pairs (lpPPIs).
599 Fraction detected, and confidence clouds (68.3% Bayesian confidence interval) were calculated at
600 each NLR score threshold. Instead of establishing a detection threshold solely reliant on the
601 hsRRS-v2 pair with the maximum NLR (Choi *et al*, 2019), we opted to derive the threshold from
602 the entire distribution of hsRRS-v2 scores. Specifically, we selected a Z-score threshold of 2.23,
603 aligning with the next non-null detection value for a dataset size of 78, corresponding to a 1/78
604 hsRRS-v2 detection rate.
605
606 *iBFG-Y2H analysis and data availability*
607 Analysis scripts, resource files, and raw data can be accessed at
608 https://github.com/EnsmingerLab/iBFG-Y2H.
609
610 **Acknowledgements**
611 We thank members of the Roth lab: Marinella Gebbia for assistance with library construction;
612 Jochen Weile, Natascha van Lieshout, Anjali Gopal, and Nozomu Yachie for bioinformatic advice.
613 Finally, we thank members of the Ensminger lab: Veronique Cartier-Archambault and Guangqi
614 Zhou for help with cloning; Beth Nicholson, Jordan Lin and John McPherson for their suggestions
615 and careful reading of the manuscript.
616

Funding

HOM was supported by a CGS-D fellowship from the Natural Sciences and Engineering Research Council of Canada. This work was supported by a Project Grant (AWE) from the Canadian Institutes of Health Research (PJT-162256). This work was supported by a Wallonia-Brussels International (WBI)-World Excellence Fellowship (FL, GC), a Fonds de la Recherche Scientifique (FRS-FNRS)-Télévie Grant (FC31747, Crédit n° 7459421F) (FL, J-CT), the Fondation Léon Fredericq (FL and J-CT), a University of Liège mobility grant (FL), a Fonds de la Recherche Scientifique (FRS-FNRS) Mobility and Congress funding (n°40020393) (FL), a Josée and Jean Schmets Prize (FL), a Herman-van Beneden Prize (FL), and a Fonds de la Recherche Scientifique (FRS-FNRS)-Fund for Research Training in Industry and Agriculture (FRIA) Grant (FC31543, Crédit n° 1E00419F) (GC). MV is a Chercheur Qualifié Honoraire and J-CT is a Maître de Recherche from the Fonds de la Recherche Scientifique (FRS-FNRS, Wallonia-Brussels Federation, Belgium). DS, AGC, NK, RL, JJK, D-KK, and FPR were supported by a Canadian Institutes of Health Research Foundation Grant (FDN159926).

Author contributions

MLU and AWE conceived and designed the screen for effector-effector interactions. HOM constructed the library and performed the iBFG-Y2H screen with assistance and training from AGC, DS, and MLU. Large-scale Gateway cloning was performed by MLU, AGC, NK, and RL, with subsequent robotic cherry-picking by AGC, NK, RL, DK and JK. Library sequencing was performed by HOM, DS, AGC, NK, and RL. HOM and MLU analyzed the data with assistance from DS. MLU performed the Y2H confirmation experiments, MOP assisted MLU with data analysis and network visualization. FL performed the yN2H validation experiment with assistance

640 from KSF. GC analyzed the yN2H data. MC, JCT, MV, FPR, and AWE provided project
641 supervision and advice. MLU and AWE prepared the manuscript with input from other authors.
642

643 ## Competing interests

644 FPR and MV are advisors and shareholders of SeqWell, Inc. (Beverly, MA, USA).
645

646 **Figure legends**

647 **Figure 1: inducible BFG-Y2H**

648 **A** Schematic representation of the iBFG-Y2H screen. 1: All AD-Y and DB-X vectors carry a
649 unique molecular barcode consisting of an uptag and a downtag of which one is flanked by lox
650 sites (*loxP*, *lox2272*; grey and black bar). 2: Haploid yeast pools with unique barcoded AD-Y and
651 DB-X clones are mated *en masse* and grown on medium lacking tryptophan and leucine to select
652 for diploid cells carrying all combinations of the AD and DB vectors. 3: The diploid pool is grown
653 on control and Y2H-selective conditions with 1 mM $CuSO_4$ to induce expression of the AD-Y and
654 DB-X fusions. AD-Y and DB-X fused proteins that interact with each other reconstitute the
655 function of the Gal4p transcription factor and drive expression of the reporter gene *GAL1::HIS3*,
656 allowing growth on Y2H selective medium. 4: After induction of Cre-recombinase expression, the
657 AD-Y downtag and DB-X uptag recombine with each other in each cell, creating two chimeric
658 barcodes that represent the combined identities of the AD-Y and DB-X vectors in those cells. 5:
659 The chimeric barcodes are PCR amplified using primers containing Illumina adaptor sequences.
660 6: Illumina sequencing gives the abundance of each unique chimeric barcode, which reflects the
661 abundance of the cells carrying those specific X-Y combinations in the control or Y2H selection

662 pool. This abundance in turn reflects, in the Y2H selection condition, the interaction between the
663 AD-Y and DB-X fusion partners.
664 **B** Test of the *CUP1* promoter in the AD and DB vectors. Empty AD and DB vectors were grown
665 on medium lacking copper and tryptophan (AD, SC-Trp) or leucine (DB, SC-Leu), backdiluted
666 and grown with and without 1 mM $CuSO_4$. Samples were taken at 0, 3, 6 and 24 h, analyzed on
667 SDS-PAGE and immunoblotted using anti-AD, anti-DB and anti-actin as a loading control.
668 **C** An inducible Y2H assay using known Y2H interaction pairs between yeast growth inhibitory *L.*
669 *pneumophila* effectors (underlined) and their antagonist metaeffectors (Urbanus *et al*, 2016) and
670 empty vector controls (EV). Strains were spotted on control (SC-Leu/Trp, selection for presence
671 of both the AD and DB vectors) or Y2H selection conditions: (SC-Leu/Trp/His + 1 mM $CuSO_4$)
672 without (low stringency) or with 1 mM 3-AT (high stringency). The non-toxic DB-fused
673 antagonist metaeffector is mated with AD empty vector to screen for autoactivation (e.g. the ability
674 to drive *GAL1::HIS3* expression by itself). Plates were incubated for 3 days at 30˚C before
675 imaging.
676
677 **Figure 2: Performance of the iBFG-Y2H *L. pneumophila* effector screen**
678 **A** Interaction score matrix of all human positive reference set (hsPRS) ORFs. The 21 expected
679 interaction pairs are highlighted in red. The interaction score heatmap is visualized using two
680 ranges, 0-1000 and 1000-31,000, to capture the entire score range.
681 **B** Mathew's correlation coefficient (MCC, black), precision (prec, green) and recall (RC, purple)
682 plot for the hsPRS. The optimal MCC is indicated with a grey line. The interaction score, precision
683 and recall values at the optimal MCC are listed.

684 **C** Bar graph showing the ranked interaction scores of the top 140 interaction pairs above the MCC-
685 optimal threshold. The panels below show the location of the human PRS (blue) and the results of
686 the iBFG-Y2H retest experiment (white - not tested, grey – negative and black – positive). To
687 confirm interaction pairs, ORFs were recloned in inducible AD or DB vectors using confirmed
688 Gateway Entry vectors and transformed to the BFG-Y2H yeast strains. Haploid strains carrying
689 the AD or DB vectors were mated and resulting diploids selected, spotted on control (SC-Leu/Trp)
690 and Y2H selective (SC-Leu/Trp/His + 1 mM $CuSO_4$) conditions and grown for 3 days at 30°C.
691 The images of the retest set are shown in Fig EV2, and the results are listed in Table EV4.
692
693 **Figure 3: Validation of the iBFG-Y2H interaction pairs by the orthologous yN2H method**
694 **A** The log-transformed normalized luminescence ratio (NLR) from the yN2H experiment is
695 plotted for a random sampling of the human PRS (hsPRS-v2), RRS (hsRRS-v2) and 33 iBFG-
696 Y2H pairs that were verified in the iBFG-Y2H retest screen (lpPPIs). The dashed line indicates
697 Log2 NLR value of 1.776 where the Z-score for the RRS is 2.23. Confidence clouds represent a
698 68.3% Bayesian confidence interval.
699 **B** The detection rate of the lpPPI, hsPRS-V2 and hsRRS-V2 based on the threshold in **A**. Error
700 bars represent a 68.3% Bayesian confidence interval. The detection rate of the *L. pneumophila*
701 pairs exceeds the detection rate of the hsPRS-V2 pairs, suggesting robustness of this interaction
702 set.
703
704 **Figure 4: iBFG-Y2H captures several interactions of the Dot/Icm complex**
705 **A** The Dot/Icm T4SS interaction score matrix showing the 27 DB- or 28 AD-fusions of the
706 Dot/Icm components present in the screen. The nine interaction pairs that were positive in the

707 iBFG-Y2H retest screen (Fig EV2) are circled in black, published interactions are indicated with
708 a star.
709 **B** Inducible Y2H assay for nine verified Dot/Icm-Dot/Icm interaction pairs on different Y2H
710 selective conditions. X-Y pairs that were positive in the retest screen (Fig EV2) were grown on
711 diploid selective medium (-Leu/Trp) and two Y2H selective conditions: the low stringency
712 condition used in the retest screen (-Leu/Trp/His + 1mM CuSO4) and a higher stringency condition
713 (-Leu/Trp/His + 1 mM CuSO4 + 1 mM 3-AT). To assay for autoactivator activity of the DB-X or
714 AD-Y fusion, each DB-X or AD-Y fusion is mated with AD or DB empty vector, respectively.
715 DB-IcmS is an autoactivator (the ability to grow on -Leu/Trp/His + 1mM $CuSO_4$ in the absence
716 of an DB-AD complex). In the higher stringency condition (-Leu/Trp/His + 1mM $CuSO_4$/ 1mM
717 3-AT), the DB-IcmS – AD-IcmW diploid can still grow, but DB-IcmS with AD-empty vector
718 diploid cannot.
719 **C** Inducible Y2H assay of verified effector-Dot/Icm interaction pairs on different Y2H-selective
720 conditions, as described above. The core effector RavC, conserved across *Legionella* species, is
721 indicated with a star.
722
723 **Figure 5: iBFG-Y2H effector-effector protein interactions**
724 **A** Inducible Y2H assay of verified interactions of effectors and putative effectors that self-interact
725 on different Y2H selective conditions. The 11 X-Y pairs that tested positive in the retest screen
726 (Fig EV2) and their AD or DB empty vector control combinations were grown on diploid selective
727 medium (-Leu/Trp) and two Y2H selective conditions: the low stringency condition used in the
728 retest screen (-Leu/Trp/His + 1mM $CuSO_4$) and a higher stringency condition (-Leu/Trp/His + 1

729 mM $CuSO_4$/1 mM 3-AT). In panel **A** and **B**, DB-Lpg2860 is an autoactivator in the low stringency
730 condition but not in the higher stringency condition.
731 **B** Inducible Y2H assay of 11 AD-DB novel pairs that were positive in the retest screen and involve
732 two effectors or putative effectors on different Y2H selective conditions, as described above. Core
733 effectors conserved in all *Legionella* species are indicated with a star.
734
735 **Figure 6: iBFG-Y2H interactions of human positive reference set proteins with effectors and**
736 **putative effectors**
737 **A** Inducible Y2H assay of verified interactions of effectors and putative effector Lpg2266 with
738 human transcription factor IKZF1 on different Y2H-selective conditions. The 8 X-Y pairs that
739 tested positive in the retest screen (Fig EV2) and their AD or DB empty vector control
740 combinations were grown on diploid selective medium (-Leu/Trp) and two Y2H selective
741 conditions: the low stringency condition used in the retest screen (-Leu/Trp/His + 1mM CuSO4)
742 and a higher stringency condition (-Leu/Trp/His + 1 mM $CuSO_4$/1 mM 3-AT). The core effector
743 LegA3 (indicated with a star) is an autoactivator on low stringency medium, but not in the higher
744 stringency condition.
745 **B** Inducible Y2H assay of 9 verified interaction pairs (Fig EV2) between effectors and several
746 proteins from the human positive reference set on different Y2H-selective conditions, as described
747 above.
748
749 **Figure 7: A network view of the iBFG-Y2H interaction pairs**
750 A network showing all the verified interaction pairs captured in the iBFG-Y2H screen involving
751 effectors or putative effectors. Effectors are shown as a rectangle, Dot/Icm components as a

752 diamond and human PRS proteins as an oval. Arrows point from DB to AD; the thickness of the
753 edges is reflective of the iBFG-Y2H interaction score. Core effectors are indicated by a star and
754 nodes of previously published PPIs are shown in blue. The network was created using Cytoscape
755 v3.101 (Shannon *et al*, 2003).
756
757 **Figure EV1: iBFG-Y2H barcode representation and correlation of fusion barcode tags**
758 **A, B** The bar graphs show the distribution of barcode representation of ORFs in the AD (**A**) and
759 DB (**B**) collection. The majority of ORFs are represented by at least three uniquely barcoded
760 vectors.
761 **C, D** Barcode recombination leads to an equal number of up and down fusion barcodes for each
762 unique pair. The scatter plots show the counts of the uptag fusion barcodes plotted against the
763 downtag fusion barcodes and the Pearson correlation (PCC) of the barcode pair abundance across
764 the entire population in the control (**C**) and Y2H selective (**D**) conditions. The uptag and downtag
765 fusions show good concordance, which indicates that there are no major barcode-specific effects
766 due to PCR or sequencing.
767
768 **Figure EV2: Retest of iBFG-Y2H interactions with *L. pneumophila* effectors**
769 All 107 interaction pairs above the optimal MCC interaction score threshold involving effectors
770 (effector-effector, effector-human, effector-Dot/Icm) and Dot/Icm-Dot/Icm pairs were retested.
771 The vectors were recloned from confirmed Gateway entry clones, transformed to BFG-Y2H strains
772 RY1010 and RY1030 and arrayed in an AD and DB array. A1 in plate 1 and 2 are empty vector
773 controls, see Table EV4 for the ORF identities in each spot.

774 **A** The DB array was mated with AD-EV, spotted on diploid selective (-Leu/Trp medium) and
775 Y2H selective conditions (-Leu/Trp/His + 1 mM $CuSO_4$) and grown for 3 days before imaging.
776 Two effector fusions (DB-Lpg2860 and DB-Lpg2300/LegA3) and one Dot/Icm fusion (DB-IcmS)
777 are autoactivators and can grow on Y2H selective conditions in the presence of the AD empty
778 vector.
779 **B** The AD array was mated with DB-EV and grown as above.
780 **C** The DB array was mated with the AD-array and grown as above. Of the 107 interaction pairs,
781 56 interactions verify in the retest experiment.
782

783 **References**

784
785

786 Bastidas RJ, Kędzior M, Davidson RK, Walsh SC, Dolat L, Sixt BS, Pruneda JN, Coers J &
787 Valdivia RH (2024) The acetylase activity of Cdu1 regulates bacterial exit from infected cells
788 by protecting Chlamydia effectors from degradation. *eLife* 12: RP87386

789 Belyi Y, Tartakovskaya D, Tais A, Fitzke E, Tzivelekidis T, Jank T, Rospert S & Aktories K
790 (2012) Elongation Factor 1A Is the Target of Growth Inhibition in Yeast Caused by
791 Legionella pneumophila Glucosyltransferase Lgt1. *J Biol Chem* 287: 26029–26037

792 Bhogaraju S, Bonn F, Mukherjee R, Adams M, Pfleiderer MM, Galej WP, Matkovic V, Lopez-
793 Mosqueda J, Kalayil S, Shin D, *et al* (2019) Inhibition of bacterial ubiquitin ligases by SidJ–
794 calmodulin catalysed glutamylation. *Nature* 572: 382–386

795 Black MH, Osinski A, Gradowski M, Servage KA, Pawłowski K, Tomchick DR & Tagliabracci
796 VS (2019) Bacterial pseudokinase catalyzes protein polyglutamylation to inhibit the SidE-
797 family ubiquitin ligases. *Science* 364: 787–792

798 Boamah DK, Zhou G, Ensminger AW & O'Connor TJ (2017) From Many Hosts, One
799 Accidental Pathogen: The Diverse Protozoan Hosts of Legionella. *Front Cell Infect Mi* 7: 477

800 Boldin MP, Mett IL & Wallach D (1995) A protein related to a proteasomal subunit binds to the
801 intracellular domain of the p55 TNF receptor upstream to its 'death domain.' *FEBS Lett* 367:
802 39–44

803 Brachmann CB, Davies A, Cost GJ, Caputo E, Li J, Hieter P & Boeke JD (1998) Designer
804 deletion strains derived from Saccharomyces cerevisiae S288C: A useful set of strains and
805 plasmids for PCR-mediated gene disruption and other applications. *Yeast* 14: 115–132

806 Braun P, Tasan M, Dreze M, Barrios-Rodiles M, Lemmens I, Yu H, Sahalie JM, Murray RR,
807 Roncari L, Smet A-S de, *et al* (2009) An experimentally derived confidence score for binary
808 protein-protein interactions. *Nat Methods* 6: 91–97

809 Bugalhão JN, Mota LJ & Franco IS (2016) Identification of regions within the Legionella
810 pneumophila VipA effector protein involved in actin binding and polymerization and in
811 interference with eukaryotic organelle trafficking. *Microbiologyopen* 5: 118–133

812 Burstein D, Amaro F, Zusman T, Lifshitz Z, Cohen O, Gilbert JA, Pupko T, Shuman HA &
813 Segal G (2016) Genomic analysis of 38 Legionella species identifies large and diverse
814 effector repertoires. *Nat Genet* 48: 167–175

815 Burstein D, Zusman T, Degtyar E, Viner R, Segal G & Pupko T (2009) Genome-Scale
816 Identification of Legionella pneumophila Effectors Using a Machine Learning Approach.
817 *Plos Pathog* 5: e1000508

818 Butt TR & Ecker DJ (1987) Yeast metallothionein and applications in biotechnology. *Microbiol*
819 *Rev* 51: 351–64

820 Camacho C, Coulouris G, Avagyan V, Ma N, Papadopoulos J, Bealer K & Madden TL (2009)
821 BLAST+: architecture and applications. *BMC Bioinform* 10: 421

822 Campodonico EM, Chesnel L & Roy CR (2005) A yeast genetic system for the identification and
823 characterization of substrate proteins transferred into host cells by the Legionella
824 pneumophila Dot/Icm system. *Mol Microbiol* 56: 918–933

825 Choi SG, Olivet J, Cassonnet P, Vidalain P-O, Luck K, Lambourne L, Spirohn K, Lemmens I,
826 Santos MD, Demeret C, *et al* (2019) Maximizing binary interactome mapping with a minimal
827 number of assays. *Nat Commun* 10: 3907

828 Chua MD, Mineva GM & Guttman JA (2023) Ube2N is present and functions within listeria
829 Actin-rich structures and lamellipodia: A localization and pharmacological inhibition study.
830 *Anat Rec* 306: 1140–1148

831 Chua MD, Moon K, Foster LJ & Guttman JA (2018) Whole cell and bacterial movement: The
832 identification of the ubiquitin E2 enzyme (Ube2N) as a novel actin-associated protein. *FASEB*
833 *J* 32: 369.4-369.4

834 Coers J, Kagan JC, Matthews M, Nagai H, Zuckman DM & Roy CR (2000) Identification of Icm
835 protein complexes that play distinct roles in the biogenesis of an organelle permissive for
836 Legionella pneumophila intracellular growth. *Mol Microbiol* 38: 719–736

837 Dean P, Mühlen S, Quitard S & Kenny B (2010) The bacterial effectors EspG and EspG2 induce
838 a destructive calpain activity that is kept in check by the co-delivered Tir effector. *Cell*
839 *Microbiol* 12: 1308–1321

840 de Felipe KS, Glover RT, Charpentier X, Anderson OR, Reyes M, Pericone CD & Shuman HA
841 (2008) Legionella Eukaryotic-Like Type IV Substrates Interfere with Organelle Trafficking.
842 *PLoS Pathog* 4: e1000117

843 Dong N, Niu M, Hu L, Yao Q, Zhou R & Shao F (2016) Modulation of membrane
844 phosphoinositide dynamics by the phosphatidylinositide 4-kinase activity of the Legionella
845 LepB effector. *Nat Microbiol* 2: 16236

846 Duménil G & Isberg RR (2001) The Legionella pneumophila IcmR protein exhibits chaperone
847 activity for IcmQ by preventing its participation in high-molecular-weight complexes. *Mol*
848 *Microbiol* 40: 1113–1127

849 Dunbar JD, Song HY, Guo D, Wu LW & Donner DB (1997) Two-hybrid cloning of a gene
850 encoding TNF receptor-associated protein 2, a protein that interacts with the intracellular
851 domain of the type 1 TNF receptor: identity with subunit 2 of the 26S protease. *J Immunol*
852 158: 4252–9

853 Durie CL, Sheedlo MJ, Chung JM, Byrne BG, Su M, Knight T, Swanson M, Lacy DB & Ohi
854 MD (2020) Structural analysis of the Legionella pneumophila Dot/Icm type IV secretion
855 system core complex. *eLife* 9: e59530

856 Ensminger AW (2016) Legionella pneumophila, armed to the hilt: justifying the largest arsenal
857 of effectors in the bacterial world. *Curr Opin Microbiol* 29: 74–80

858 Faulkner G, Berk SG, Garduño E, Ortiz-Jiménez MA & Garduño RA (2008) Passage through
859 Tetrahymena tropicalis Triggers a Rapid Morphological Differentiation in Legionella
860 pneumophila. *J Bacteriol* 190: 7728–7738

861 Fields BS (1996) The molecular ecology of legionellae. *Trends Microbiol* 4: 286–290

862 Fields BS, Benson RF & Besser RE (2002) Legionella and Legionnaires' Disease: 25 Years of
863 Investigation. *Clin Microbiol Rev* 15: 506–526

864 Fields S & Song O (1989) A novel genetic system to detect protein–protein interactions. *Nature*
865 340: 245–246

866 Finsel I & Hilbi H (2015) Formation of a pathogen vacuole according to Legionella
867 pneumophila: how to kill one bird with many stones. *Cell Microbiol* 17: 935–950

868 Franco IS, Shohdy N & Shuman HA (2012) The Legionella pneumophila Effector VipA Is an
869 Actin Nucleator That Alters Host Cell Organelle Trafficking. *Plos Pathog* 8: e1002546

870 Gan N, Guan H, Huang Y, Yu T, Fu J, Nakayasu ES, Puvar K, Das C, Wang D, Ouyang S, *et al*
871 (2020) Legionella pneumophila regulates the activity of UBE2N by deamidase-mediated
872 deubiquitination. *Embo J* 39: e102806

873 Gan N, Nakayasu ES, Hollenbeck PJ & Luo Z-Q (2019a) Legionella pneumophila inhibits
874 immune signalling via MavC-mediated transglutaminase-induced ubiquitination of UBE2N.
875 *Nat Microbiol* 4: 134–143

876 Gan N, Zhen X, Liu Y, Xu X, He C, Qiu J, Liu Y, Fujimoto GM, Nakayasu ES, Zhou B, *et al*
877 (2019b) Regulation of phosphoribosyl ubiquitination by a calmodulin-dependent glutamylase.
878 *Nature* 572: 387–391

879 Ge J, Xu H, Li T, Zhou Y, Zhang Z, Li S, Liu L & Shao F (2009) A Legionella type IV effector
880 activates the NF-κB pathway by phosphorylating the IκB family of inhibitors. *Proc National*
881 *Acad Sci* 106: 13725–13730

882 Ghosal D, Jeong KC, Chang Y-W, Gyore J, Teng L, Gardner A, Vogel JP & Jensen GJ (2019)
883 Molecular architecture, polar targeting and biogenesis of the Legionella Dot/Icm T4SS. *Nat*
884 *Microbiol* 4: 1173–1182

885 Gietz RD & Schiestl RH (2007a) Frozen competent yeast cells that can be transformed with high
886 efficiency using the LiAc/SS carrier DNA/PEG method. *Nat Protoc* 2: 1–4

887 Gietz RD & Schiestl RH (2007b) High-efficiency yeast transformation using the LiAc/SS carrier
888 DNA/PEG method. *Nat Protoc* 2: 31–34

889 Gomez-Valero L, Rusniok C, Carson D, Mondino S, Pérez-Cobas AE, Rolando M, Pasricha S,
890 Reuter S, Demirtas J, Crumbach J, *et al* (2019) More than 18,000 effectors in the Legionella
891 genus genome provide multiple, independent combinations for replication in human cells.
892 *Proc Natl Acad Sci* 116: 2265–2273

893 Guo Z, Stephenson R, Qiu J, Zheng S & Luo Z-Q (2014) A Legionella effector modulates host
894 cytoskeletal structure by inhibiting actin polymerization. *Microbes Infect* 16: 225–236

895 He L, Lin Y, Ge Z, He S, Zhao B, Shen D, He J & Lu Y (2019) The Legionella pneumophila
896 effector WipA disrupts host F-actin polymerisation by hijacking phosphotyrosine signalling.
897 *Cell Microbiol* 21: e13014

898 Heidtman M, Chen EJ, Moy M & Isberg RR (2009) Large-scale identification of Legionella
899 pneumophila Dot/Icm substrates that modulate host cell vesicle trafficking pathways. *Cell*
900 *Microbiol* 11: 230–248

901 Hervet E, Charpentier X, Vianney A, Lazzaroni J-C, Gilbert C, Atlan D & Doublet P (2011)
902 Protein Kinase LegK2 Is a Type IV Secretion System Effector Involved in Endoplasmic
903 Reticulum Recruitment and Intracellular Replication of Legionella pneumophila. *Infect*
904 *Immun* 79: 1936–1950

905 Hsieh T-S, Lopez VA, Black MH, Osinski A, Pawłowski K, Tomchick DR, Liou J &
906 Tagliabracci VS (2021) Dynamic remodeling of host membranes by self-organizing bacterial
907 effectors. *Science* 372: 935–941

908 Huang L, Boyd D, Amyot WM, Hempstead AD, Luo Z, O'Connor TJ, Chen C, Machner M,
909 Montminy T & Isberg RR (2011) The E Block motif is associated with Legionella
910 pneumophila translocated substrates. *Cell Microbiol* 13: 227–245

911 Isberg RR, O'Connor TJ & Heidtman M (2009) The Legionella pneumophila replication
912 vacuole: making a cosy niche inside host cells. *Nat Rev Microbiol* 7: 13–24

913 Jeong KC, Sexton JA & Vogel JP (2015) Spatiotemporal Regulation of a Legionella
914 pneumophila T4SS Substrate by the Metaeffector SidJ. *Plos Pathog* 11: e1004695

915 Jia Q, Lin Y, Gou X, He L, Shen D, Chen D, Xie W & Lu Y (2018) Legionella pneumophila
916 effector WipA, a bacterial PPP protein phosphatase with PTP activity. *Acta Biochim Biophys*
917 *Sin* 50: 547–554

918 Joseph AM, Pohl AE, Ball TJ, Abram TG, Johnson DK, Geisbrecht BV & Shames SR (2020)
919 The Legionella pneumophila Metaeffector Lpg2505 (MesI) Regulates SidI-Mediated
920 Translation Inhibition and Novel Glycosyl Hydrolase Activity. *Infect Immun* 88: e00853-19

921 Joseph AM & Shames SR (2021) Affecting the Effectors: Regulation of Legionella pneumophila
922 Effector Function by Metaeffectors. *Pathogens* 10: 108

923 Kim H, Kubori T, Yamazaki K, Kwak M-J, Park S-Y, Nagai H, Vogel JP & Oh B-H (2020)
924 Structural basis for effector protein recognition by the Dot/Icm Type IVB coupling protein
925 complex. *Nat Commun* 11: 2623

926 Kubori T & Galán JE (2003) Temporal Regulation of Salmonella Virulence Effector Function by
927 Proteasome-Dependent Protein Degradation. *Cell* 115: 333–342

928 Kubori T & Nagai H (2011) Bacterial Effector-Involved Temporal and Spatial Regulation by
929 Hijack of the Host Ubiquitin Pathway. *Front Microbiol* 2: 145

930 Kubori T, Shinzawa N, Kanuka H & Nagai H (2010) Legionella Metaeffector Exploits Host
931 Proteasome to Temporally Regulate Cognate Effector. *Plos Pathog* 6: e1001216

932 Kuehn HS, Boast B & Rosenzweig SD (2022) Inborn errors of human IKAROS: LOF and GOF
933 variants associated with primary immunodeficiency. *Clin Exp Immunol* 212: 129–136

934 Kwak M-J, Kim JD, Kim H, Kim C, Bowman JW, Kim S, Joo K, Lee J, Jin KS, Kim Y-G, *et al*
935 (2017) Architecture of the type IV coupling protein complex of Legionella pneumophila. *Nat*
936 *Microbiol* 2: 17114

937 Langmead B & Salzberg SL (2012) Fast gapped-read alignment with Bowtie 2. *Nat Methods* 9:
938 357–359

939 Larson CL, Beare PA, Howe D & Heinzen RA (2013) Coxiella burnetii effector protein subverts
940 clathrin-mediated vesicular trafficking for pathogen vacuole biogenesis. *Proc National Acad*
941 *Sci* 110: E4770–E4779

942 Lesser CF & Miller SI (2001) Expression of microbial virulence proteins in Saccharomyces
943 cerevisiae models mammalian infection. *EMBO J* 20: 1840–1849

944 Liu M, Conover GM & Isberg RR (2008) Legionella pneumophila EnhC is required for efficient
945 replication in tumour necrosis factor α-stimulated macrophages. *Cell Microbiol* 10: 1906–
946 1923

947 Liu Y, Zhu W, Tan Y, Nakayasu ES, Staiger CJ & Luo Z-Q (2017) A Legionella Effector
948 Disrupts Host Cytoskeletal Structure by Cleaving Actin. *PLoS Pathog* 13: e1006186

949 Losick VP, Haenssler E, Moy M & Isberg RR (2010) LnaB: a Legionella pneumophila activator
950 of NF-κB. *Cell Microbiol* 12: 1083–1097

951 Luck K, Kim D-K, Lambourne L, Spirohn K, Begg BE, Bian W, Brignall R, Cafarelli T,
952 Campos-Laborie FJ, Charloteaux B, *et al* (2020) A reference map of the human binary protein
953 interactome. *Nature* 580: 402–408

954 Luo Z-Q & Isberg RR (2004) Multiple substrates of the Legionella pneumophila Dot/Icm system
955 identified by interbacterial protein transfer. *P Natl Acad Sci Usa* 101: 841–846

956 Magori S & Citovsky V (2011) Agrobacterium Counteracts Host-Induced Degradation of Its
957 Effector F-Box Protein. *Sci Signal* 4: ra69

958 McCloskey A, Perri K, Chen T, Han A & Luo Z-Q (2021) The metaeffector MesI regulates the
959 activity of the Legionella effector SidI through direct protein–protein interactions. *Microbes*
960 *Infect* 23: 104794

961 Meir A, Chetrit D, Liu L, Roy CR & Waksman G (2018) Legionella DotM structure reveals a
962 role in effector recruiting to the Type 4B secretion system. *Nat Commun* 9: 507

963 Meir A, Macé K, Lukoyanova N, Chetrit D, Hospenthal MK, Redzej A, Roy C & Waksman G
964 (2020) Mechanism of effector capture and delivery by the type IV secretion system from
965 Legionella pneumophila. *Nat Commun* 11: 2864

966 Mengue L, Régnacq M, Aucher W, Portier E, Héchard Y & Samba-Louaka A (2016) Legionella
967 pneumophila prevents proliferation of its natural host Acanthamoeba castellanii. *Sci Rep* 6:
968 36448

969 Michard C, Sperandio D, Baïlo N, Pizarro-Cerdá J, LeClaire L, Chadeau-Argaud E, Pombo-
970 Grégoire I, Hervet E, Vianney A, Gilbert C, *et al* (2015) The Legionella Kinase LegK2
971 Targets the ARP2/3 Complex To Inhibit Actin Nucleation on Phagosomes and Allow
972 Bacterial Evasion of the Late Endocytic Pathway. *Mbio* 6: e00354-15

973 Molmeret M, Horn M, Wagner M, Santic M & Kwaik YA (2005) Amoebae as Training Grounds
974 for Intracellular Bacterial Pathogens. *Appl Environ Microbiol* 71: 20–28

975 Mount HO, Zangari F, Gingras A-C & Ensminger AW (2022) The L. pneumophila effector PieF
976 modulates mRNA stability through association with eukaryotic CCR4-NOT. *Biorxiv*:
977 2022.06.06.494580

978 Mukherjee S, Liu X, Arasaki K, McDonough J, Galán JE & Roy CR (2011) Modulation of Rab
979 GTPase function by a protein phosphocholine transferase. *Nature* 477: 103–106

980 Müller MP, Peters H, Blümer J, Blankenfeldt W, Goody RS & Itzen A (2010) The *Legionella*
981 Effector Protein DrrA AMPylates the Membrane Traffic Regulator Rab1b. *Science* 329: 946–
982 949

983 Neunuebel MR, Chen Y, Gaspar AH, Backlund PS, Yergey A & Machner MP (2011) De-
984 AMPylation of the Small GTPase Rab1 by the Pathogen Legionella pneumophila. *Science*
985 333: 453–456

986 Nevo O, Zusman T, Rasis M, Lifshitz Z & Segal G (2014) Identification of Legionella
987 pneumophila Effectors Regulated by the LetAS-RsmYZ-CsrA Regulatory Cascade, Many of
988 Which Modulate Vesicular Trafficking. *J Bacteriol* 196: 681–692

989 Ninio S, Zuckman-Cholon DM, Cambronne ED & Roy CR (2005) The Legionella IcmS–IcmW
990 protein complex is important for Dot/Icm-mediated protein translocation. *Mol Microbiol* 55:
991 912–926

992 Oh K-S, Gottschalk RA, Lounsbury NW, Sun J, Dorrington MG, Baek S, Sun G, Wang Z,
993 Krauss KS, Milner JD, *et al* (2018) Dual Roles for Ikaros in Regulation of Macrophage
994 Chromatin State and Inflammatory Gene Expression. *J Immunol* 201: 757–771

995 Pinotsis N & Waksman G (2017) Structure of the WipA protein reveals a novel tyrosine protein
996 phosphatase effector from Legionella pneumophila. *J Biol Chem* 292: 9240–9251

997 Pollock TY, Marrero VRV, Brodsky IE & Shin S (2023) TNF licenses macrophages to undergo
998 rapid caspase-1, -11, and -8-mediated cell death that restricts Legionella pneumophila
999 infection. *PLOS Pathog* 19: e1010767

1000 Rao C, Benhabib H & Ensminger AW (2013) Phylogenetic Reconstruction of the Legionella
1001 pneumophila Philadelphia-1 Laboratory Strains through Comparative Genomics. *Plos One* 8:
1002 e64129

1003 Rolland T, Taşan M, Charloteaux B, Pevzner SJ, Zhong Q, Sahni N, Yi S, Lemmens I,
1004 Fontanillo C, Mosca R, *et al* (2014) A Proteome-Scale Map of the Human Interactome
1005 Network. *Cell* 159: 1212–1226

1006 Rowbotham TJ (1980) Preliminary report on the pathogenicity of Legionella pneumophila for
1007 freshwater and soil amoebae. *J Clin Pathol* 33: 1179–83

1008 Rual J-F, Venkatesan K, Hao T, Hirozane-Kishikawa T, Dricot A, Li N, Berriz GF, Gibbons FD,
1009 Dreze M, Ayivi-Guedehoussou N, *et al* (2005) Towards a proteome-scale map of the human
1010 protein–protein interaction network. *Nature* 437: 1173–1178

1011 Schator D, Mondino S, Berthelet J, Silvestre CD, Assaya MB, Rusniok C, Rodrigues-Lima F,
1012 Wehenkel A, Buchrieser C & Rolando M (2023) Legionella para-effectors target chromatin
1013 and promote bacterial replication. *Nat Commun* 14: 2154

1014 Sexton JA, Pinkner JS, Roth R, Heuser JE, Hultgren SJ & Vogel JP (2004) The Legionella
1015 pneumophila PilT Homologue DotB Exhibits ATPase Activity That Is Critical for
1016 Intracellular Growth. *J Bacteriol* 186: 1658–1666

1017 Shames SR & Finlay BB (2012) Bacterial effector interplay: a new way to view effector
1018 function. *Trends Microbiol* 20: 214–219

1019 Shames SR, Liu L, Havey JC, Schofield WB, Goodman AL & Roy CR (2017) Multiple
1020 Legionella pneumophila effector virulence phenotypes revealed through high-throughput
1021 analysis of targeted mutant libraries. *Proc National Acad Sci* 114: E10446–E10454

1022 Shannon P, Markiel A, Ozier O, Baliga NS, Wang JT, Ramage D, Amin N, Schwikowski B &
1023 Ideker T (2003) Cytoscape: A Software Environment for Integrated Models of Biomolecular
1024 Interaction Networks. *Genome Res* 13: 2498–2504

1025 Shen X, Banga S, Liu Y, Xu L, Gao P, Shamovsky I, Nudler E & Luo Z (2009) Targeting
1026 eEF1A by a Legionella pneumophila effector leads to inhibition of protein synthesis and
1027 induction of host stress response. *Cell Microbiol* 11: 911–926

1028 Shi X, Halder P, Yavuz H, Jahn R & Shuman HA (2016) Direct targeting of membrane fusion by
1029 SNARE mimicry: Convergent evolution of Legionella effectors. *Proc National Acad Sci* 113:
1030 8807–8812

1031 Shohdy N, Efe JA, Emr SD & Shuman HA (2005) Pathogen effector protein screening in yeast
1032 identifies Legionella factors that interfere with membrane trafficking. *P Natl Acad Sci Usa*
1033 102: 4866–4871

1034 Siddiqui R, Makhlouf Z & Khan NA (2021) The increasing importance of Vermamoeba
1035 vermiformis. *J Eukaryot Microbiol* 68: e12857

1036 Simonis N, Rual J-F, Carvunis A-R, Tasan M, Lemmens I, Hirozane-Kishikawa T, Hao T,
1037 Sahalie JM, Venkatesan K, Gebreab F, *et al* (2009) Empirically controlled mapping of the
1038 Caenorhabditis elegans protein-protein interactome network. *Nat Methods* 6: 47–54

1039 Sol A, Lipo E, Jesús-Díaz DA de, Murphy C, Devereux M & Isberg RR (2019) Legionella
1040 pneumophila translocated translation inhibitors are required for bacterial-induced host cell
1041 cycle arrest. *Proc Natl Acad Sci* 116: 3221–3228

1042 Song L, Xie Y, Li C, Wang L, He C, Zhang Y, Yuan J, Luo J, Liu X, Xiu Y, *et al* (2021) The
1043 Legionella Effector SdjA Is a Bifunctional Enzyme That Distinctly Regulates Phosphoribosyl
1044 Ubiquitination. *Mbio* 12: e02316-21

1045 Sutherland MC, Binder KA, Cualing PY & Vogel JP (2013) Reassessing the Role of DotF in the
1046 Legionella pneumophila Type IV Secretion System. *Plos One* 8: e65529

1047 Sutherland MC, Nguyen TL, Tseng V & Vogel JP (2012) The Legionella IcmSW Complex
1048 Directly Interacts with DotL to Mediate Translocation of Adaptor-Dependent Substrates. *Plos*
1049 *Pathog* 8: e1002910

1050 Tan Y, Arnold RJ & Luo Z-Q (2011) Legionella pneumophila regulates the small GTPase Rab1
1051 activity by reversible phosphorylcholination. *Proc National Acad Sci* 108: 21212–21217

1052 Tan Y & Luo Z-Q (2011) Legionella pneumophila SidD is a deAMPylase that modifies Rab1.
1053 *Nature* 475: 506–509

1054 Urbanus ML, Quaile AT, Stogios PJ, Morar M, Rao C, Leo RD, Evdokimova E, Lam M, Oatway
1055 C, Cuff ME, *et al* (2016) Diverse mechanisms of metaeffector activity in an intracellular
1056 bacterial pathogen, Legionella pneumophila. *Mol Syst Biol* 12: 893

1057 Valleau D, Quaile AT, Cui H, Xu X, Evdokimova E, Chang C, Cuff ME, Urbanus ML,
1058 Houliston S, Arrowsmith CH, *et al* (2018) Discovery of Ubiquitin Deamidases in the
1059 Pathogenic Arsenal of Legionella pneumophila. *Cell Reports* 23: 568–583

1060 Venkatesan K, Rual J-F, Vazquez A, Stelzl U, Lemmens I, Hirozane-Kishikawa T, Hao T,
1061 Zenkner M, Xin X, Goh K-I, *et al* (2009) An empirical framework for binary interactome
1062 mapping. *Nat Methods* 6: 83–90

1063 Vincent CD, Friedman JR, Jeong KC, Buford EC, Miller JL & Vogel JP (2006) Identification of
1064 the core transmembrane complex of the Legionella Dot/Icm type IV secretion system. *Mol*
1065 *Microbiol* 62: 1278–1291

1066 Vincent CD, Friedman JR, Jeong KC, Sutherland MC & Vogel JP (2012) Identification of the
1067 DotL coupling protein subcomplex of the Legionella Dot/Icm type IV secretion system. *Mol*
1068 *Microbiol* 85: 378–391

1069 Vincent CD & Vogel JP (2006) The Legionella pneumophila IcmS–LvgA protein complex is
1070 important for Dot/Icm-dependent intracellular growth. *Mol Microbiol* 61: 596–613

1071 Wan M, Sulpizio AG, Akturk A, Beck WHJ, Lanz M, Faça VM, Smolka MB, Vogel JP & Mao
1072 Y (2019) Deubiquitination of phosphoribosyl-ubiquitin conjugates by phosphodiesterase-
1073 domain–containing Legionella effectors. *Proc National Acad Sci* 116: 23518–23526

1074 Wang Y, Zhan Q, Wang X, Li P, Liu S, Gao G & Gao P (2020) Insights into catalysis and
1075 regulation of non-canonical ubiquitination and deubiquitination by bacterial deamidase
1076 effectors. *Nat Commun* 11: 2751

1077 Watanabe K, Nakao R, Fujishima M, Tachibana M, Shimizu T & Watarai M (2016) Ciliate
1078 Paramecium is a natural reservoir of Legionella pneumophila. *Sci Rep* 6: 24322

1079 Xu J, Xu D, Wan M, Yin L, Wang X, Wu L, Liu Y, Liu X, Zhou Y & Zhu Y (2017) Structural
1080 insights into the roles of the IcmS–IcmW complex in the type IVb secretion system of
1081 Legionella pneumophila. *Proc National Acad Sci* 114: 13543–13548

1082 Xu L, Shen X, Bryan A, Banga S, Swanson MS & Luo Z-Q (2010) Inhibition of Host Vacuolar
1083 H+-ATPase Activity by a Legionella pneumophila Effector. *PLoS Pathog* 6: e1000822

1084 Yachie N, Petsalaki E, Mellor JC, Weile J, Jacob Y, Verby M, Ozturk SB, Li S, Cote AG, Mosca
1085 R, *et al* (2016) Pooled-matrix protein interaction screens using Barcode Fusion Genetics. *Mol*
1086 *Syst Biol* 12: 863

1087 Yu H, Braun P, Yıldırım MA, Lemmens I, Venkatesan K, Sahalie J, Hirozane-Kishikawa T,
1088 Gebreab F, Li N, Simonis N, *et al* (2008) High-Quality Binary Protein Interaction Map of the
1089 Yeast Interactome Network. *Science* 322: 104–110

1090 Zhang T, Lei J, Yang H, Xu K, Wang R & Zhang Z (2011) An improved method for whole
1091 protein extraction from yeast Saccharomyces cerevisiae. *Yeast* 28: 795–798

1092 Zhu W, Banga S, Tan Y, Zheng C, Stephenson R, Gately J & Luo Z-Q (2011) Comprehensive
1093 Identification of Protein Substrates of the Dot/Icm Type IV Transporter of Legionella
1094 pneumophila. *Plos One* 6: e17638

1095

Figure 1 - Inducible BFG-Y2H

A Step 1: clone each ORF into a vector with a unique AD or DB tag.

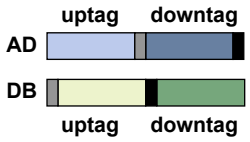

Step 2: mate pools of tagged strains.

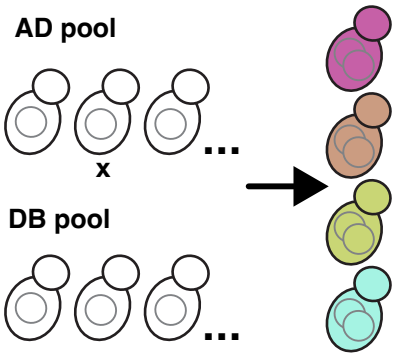

Step 3: grow diploid pool with induction.

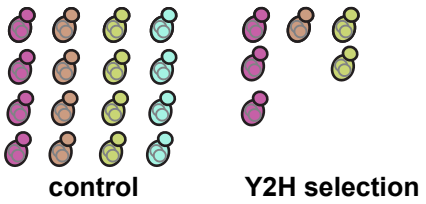

Step 4. recombine up and down tags *in vivo* (in surviving cells).

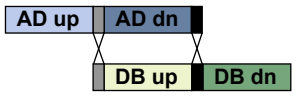

Step 5: PCR amplify fused tags.

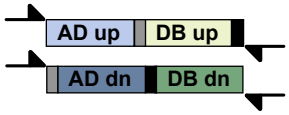

Step 6. Illumina sequence fused tags.

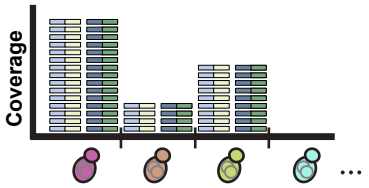

B

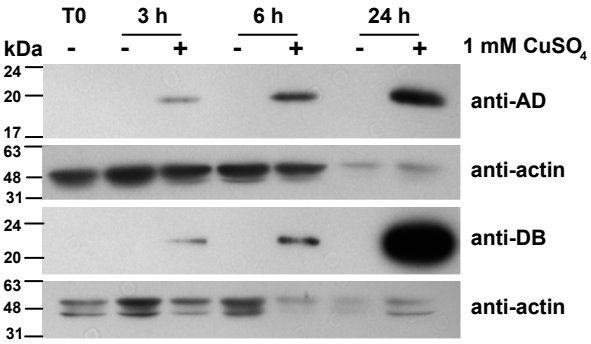

C

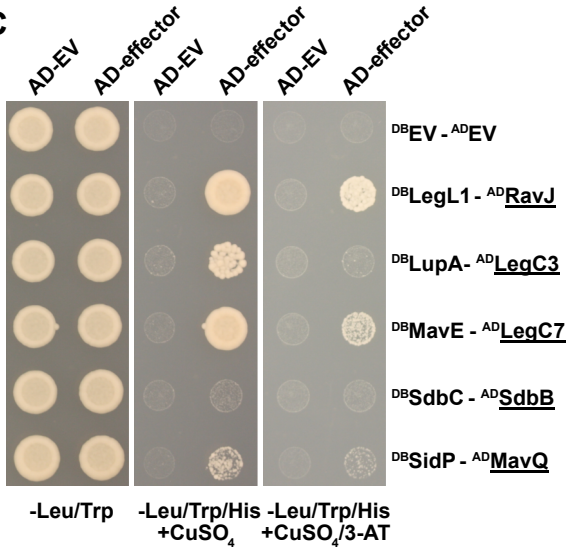

Figure 2 - Performance of the iBFG-Y2H *L. pneumophila* effector screen

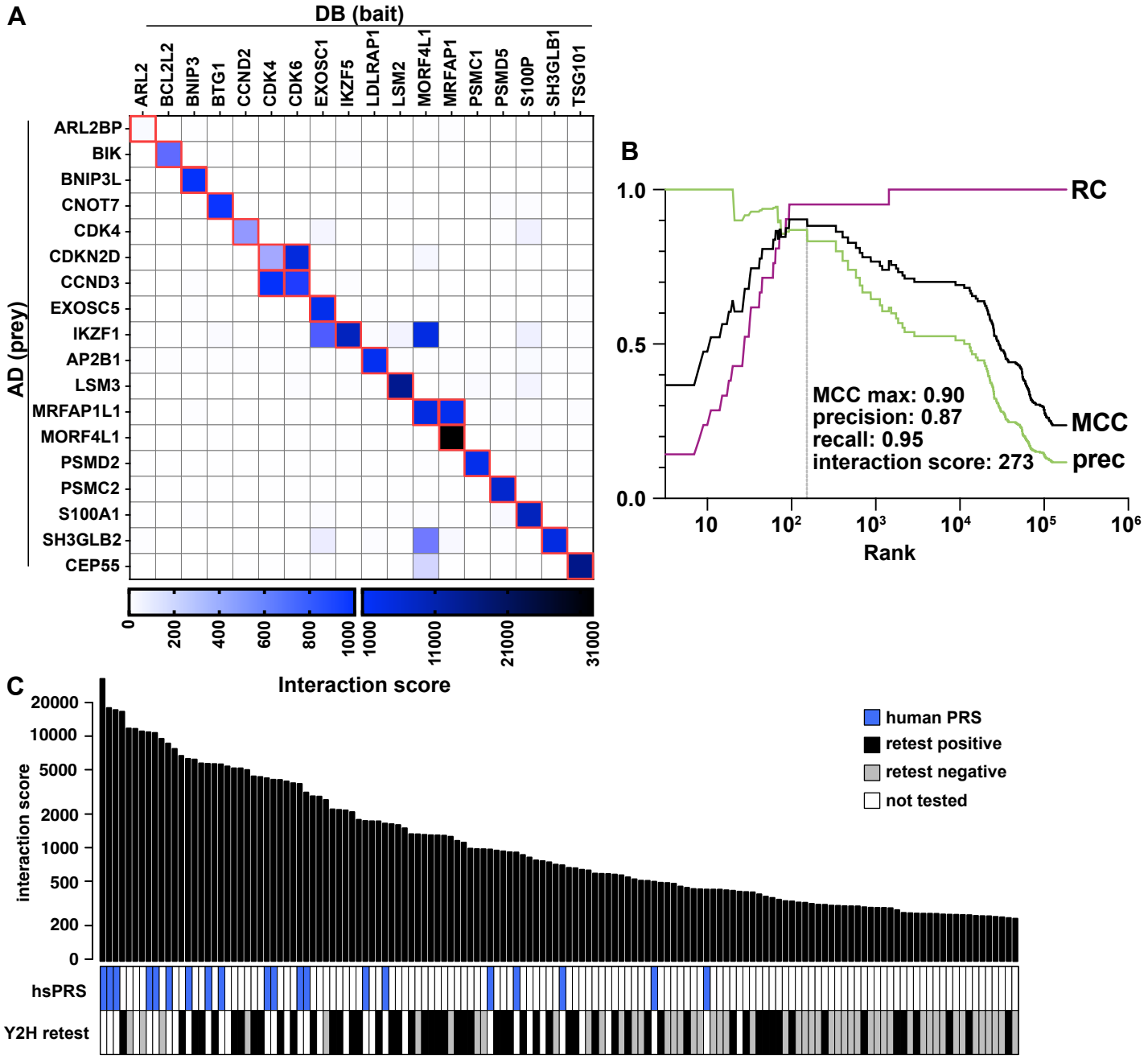

Figure 3 - Validation of the iBFG-Y2H interaction pairs by the orthologous yN2H method

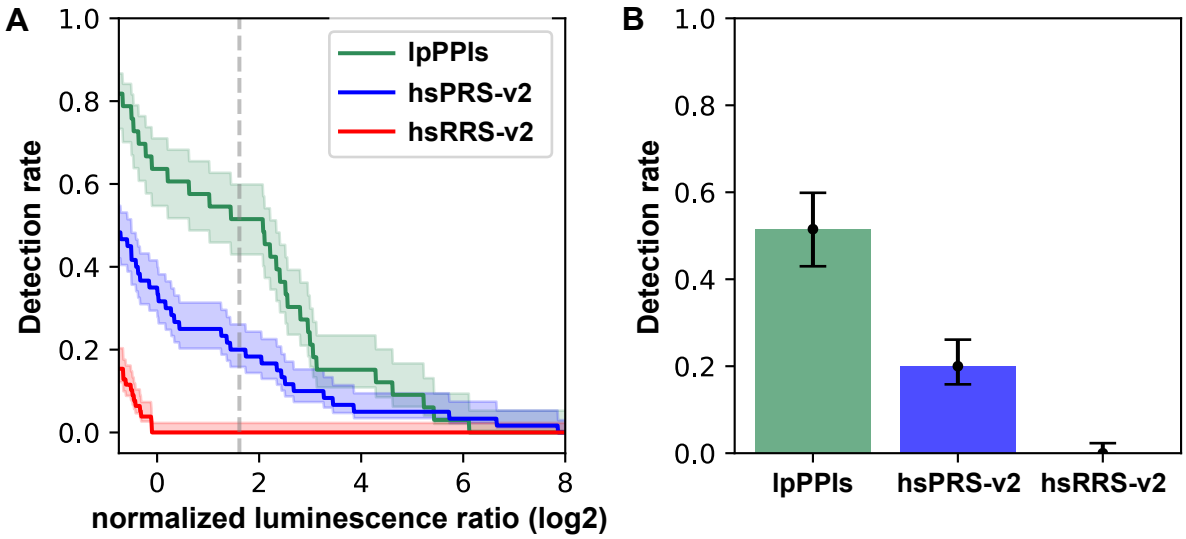

Figure 4 iBFG-Y2H captures several interactions of the Dot/Icm complex

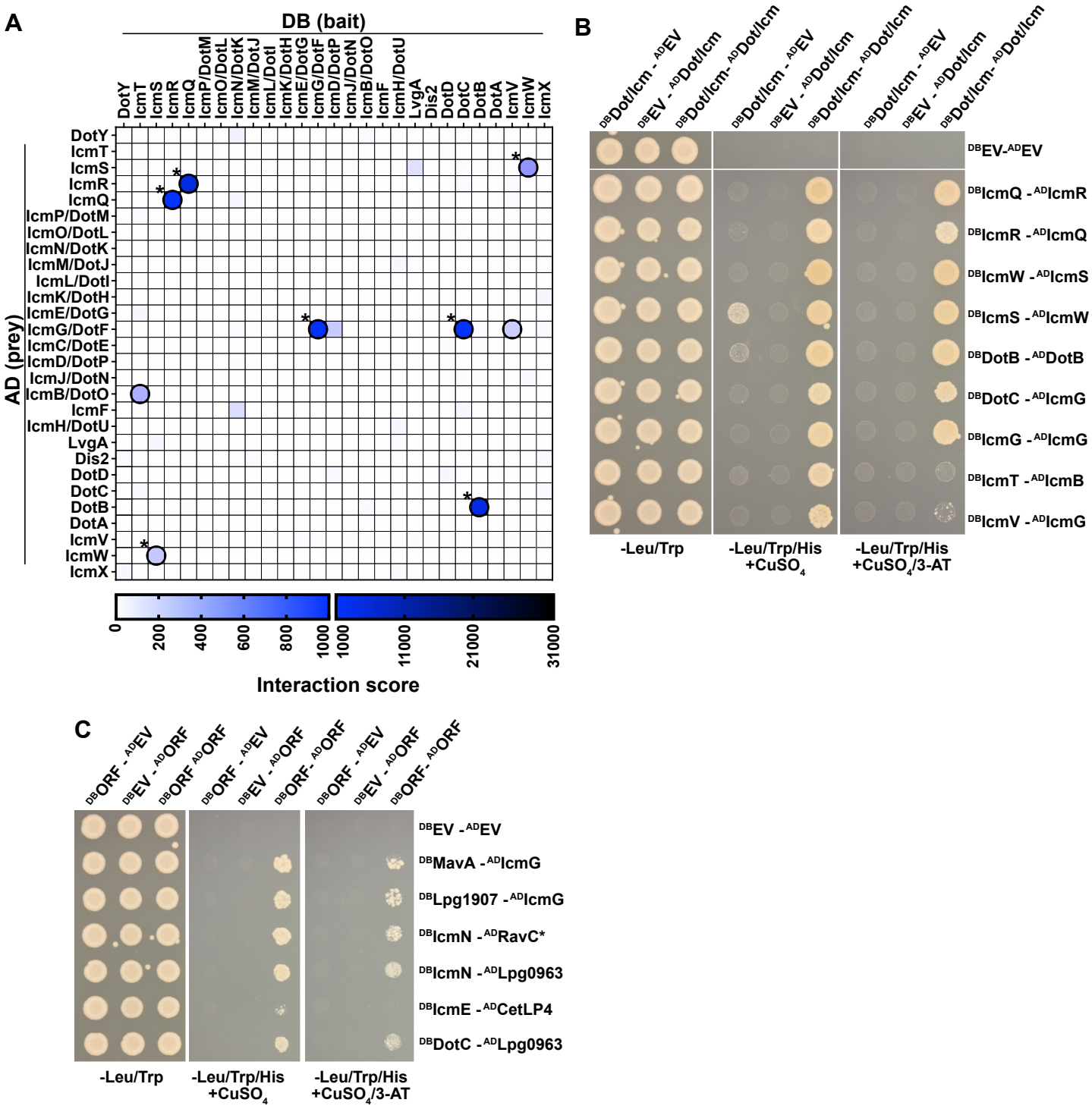

Figure 5 - iBFG-Y2H effector-effector protein interactions

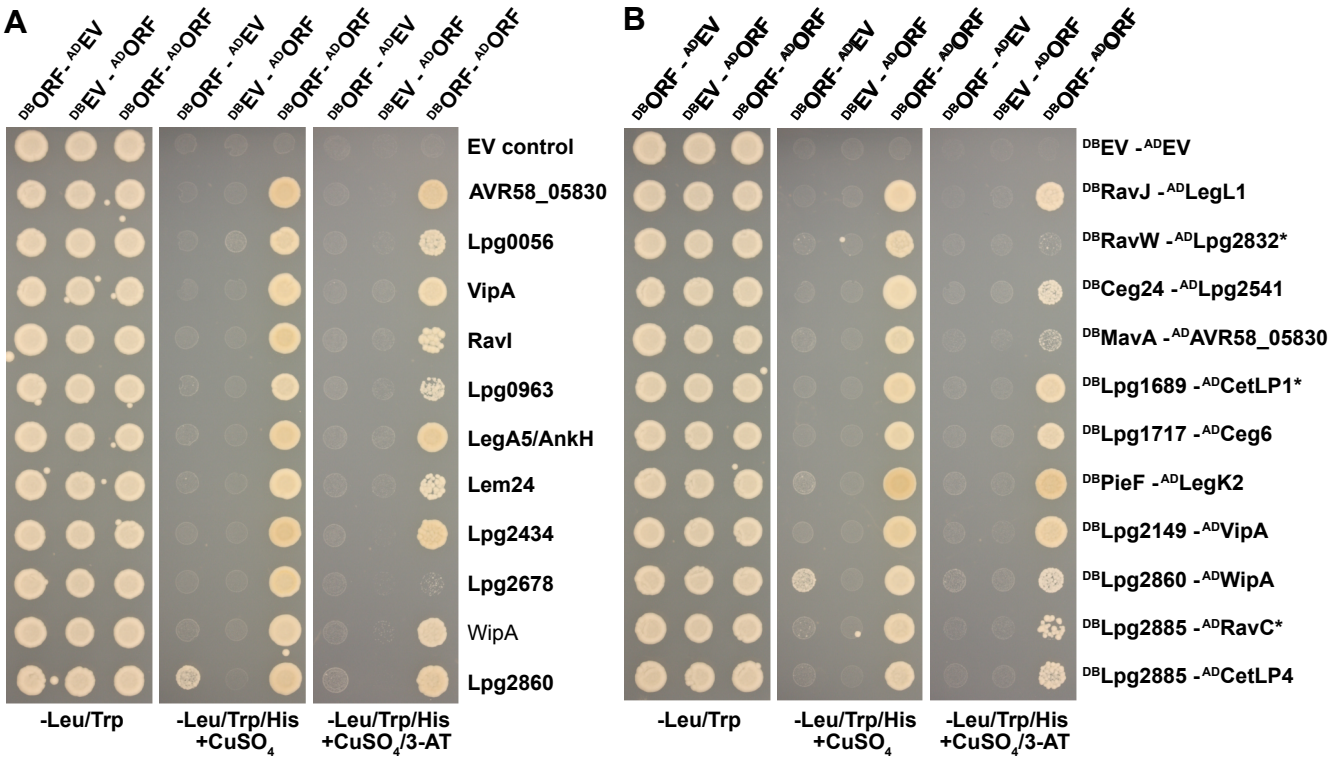

Figure 6 - iBFG-Y2H interactions of human PRS proteins with effectors and putative effectors

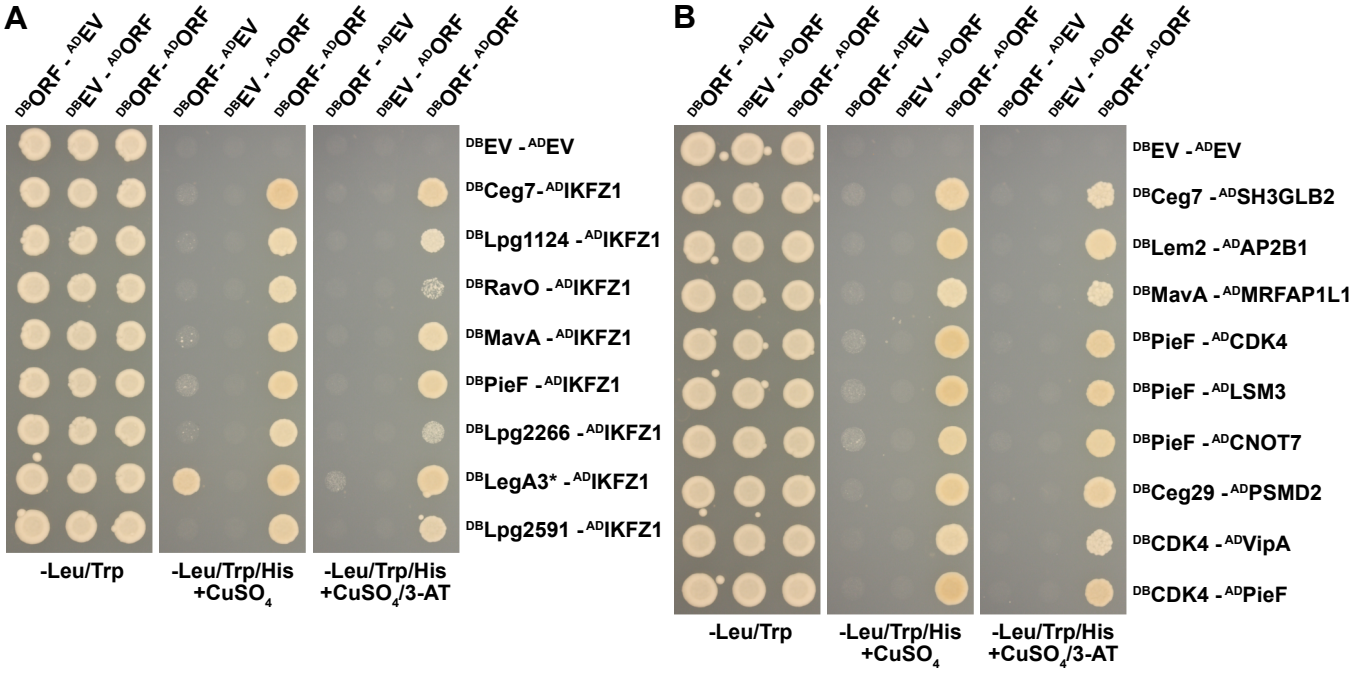
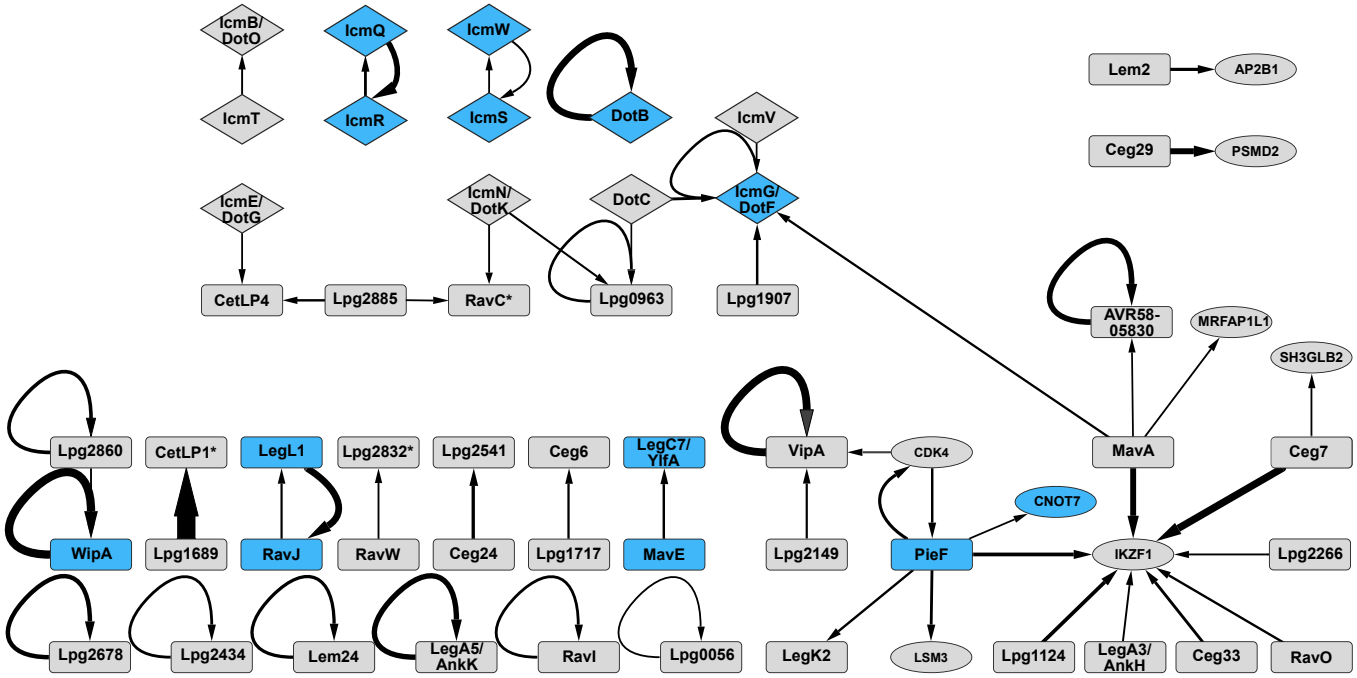
Figure 7 - A network view of the effector interaction pairs